



Originally published as:

Zang, A., Zimmermann, G., Hofmann, H., Stephansson, O., Min, K.-B., Kim, K. Y. (2019): How to Reduce Fluid-Injection-Induced Seismicity. - *Rock Mechanics and Rock Engineering*, 52, 2, pp. 475—493.

DOI: <http://doi.org/10.1007/s00603-018-1467-4>

How to reduce fluid-injection induced seismicity.

Arno Zang^{*a}, Günter Zimmermann^b, Hannes Hofmann^b, Ove Stephansson^a, Ki-Bok Min^c and Kwang Yeom Kim^d

^a Section 2.6 Seismic Hazard and Risk Dynamics, GFZ - German Research Centre for Geosciences, Telegrafenberg, Potsdam 14473, Germany

^b Section 6.2 Geothermal Energy Systems, GFZ - German Research Centre for Geosciences, Telegrafenberg, Potsdam 14473, Germany

^c Department of Energy Resources Engineering and Research Institute of Energy Resources, Seoul National University, South Korea

^d Korea Institute of Civil Engineering and Building Technology (KICT), Goyang, South Korea

Abstract

The recent growth in energy technologies and the management of subsurface reservoirs has led to increased human interaction with the Earth's crust. One consequence of this is the overall increase of anthropogenic earthquakes. To manage fluid-injection induced seismicity, in this study we propose to use an advanced fluid-injection scheme. First, long-term fluid-injection experiments are separated from short-term fluid-injection experiments. Of the short-term experiments, enhanced geothermal systems stimulations have shown a higher propensity to produce larger seismic events compared to hydraulic fracturing in oil and gas. Among the factors discussed for influencing the likelihood of an induced seismic event to occur are injection rate, cumulative injected volume, wellhead pressure, injection depth, stress state, rock type and proximity to faults. We present and discuss the concept of fatigue hydraulic fracturing at different scales in geothermal applications. In contrast to conventional hydraulic fracturing with monotonic injection of high pressure fluids, in fatigue hydraulic fracturing, the fluid is injected in pressure cycles with increasing target pressure, separated by depressurization phases for relaxing the crack tip stresses. During pressurization phases, the target pressure level is modified by pulse hydraulic fracturing generated with a second pump system. This combination of two pumps with multiple flow rates may allow a more complex fracture pattern to be designed, with arresting and branching fractures, forming a broader fracture process zone. Small scale laboratory fluid-injection tests on granite cores and intermediate-scale fluid-injection experiments in a hard rock underground laboratory are described. At laboratory scale, cyclic fluid injection test with acoustic emission analysis are reported with subsequent X-ray CT fracture pattern analysis. At intermediate-scale, in a controlled underground experiment at constant depth with well-known stress state in granitic rock, we test advanced fluid injection schemes. The goal is to optimize the fracture network and mitigate larger seismic events. General findings in granitic rock, independent of scale, are summarized. First, the fracture breakdown pressure in fatigue hydraulic testing is lower than that in conventional hydraulic fracturing. Second, compared to continuous injection the magnitude of the largest induced seismic event seems to be systematically reduced by cyclic injection. Third, the fracture pattern in fatigue testing is different from that in conventional injection tests at high pressures. Cyclic fracture pattern seem to result from chiefly generated low energy grain boundary cracks forming a wider process zone. Fourth, cyclic injection increases the permeability of the system. A combination of cyclic progressive and pulse pressurization leads to the best hydraulic performance of all schemes tested. One advantage of fatigue testing is the fact that this soft stimulation method can be applied in circumstances where conventional stimulation might otherwise be abandoned based on site-specific seismic hazard estimates.

Keywords: Crack tip stresses; Fluid-injection induced seismicity; Fracture process zone; Hydraulic fracturing.

* Corresponding author. Tel.: +49 331 288 1325

E-mail address: zang@gfz-potsdam.de

List of abbreviations and symbols

| | |
|--------------|---|
| CHF | Cyclic hydraulic fracturing |
| EGS | Enhanced geothermal system |
| FBP | Fracture breakdown pressure |
| FHF | Fatigue hydraulic fracturing |
| FIP | Fracture initiation pressure |
| FPP | Fracture propagation pressure |
| FPZ | Fracture process zone |
| ISRM | International Society for Rock Mechanics and Rock Engineering |
| PHF | Pulse hydraulic fracturing |
| RFP | Re-fracturing pressure or reopening pressure |
| ISIP | Instantaneous shut-in pressure |
| dc/dt | Crack growth rate |
| dc/dN | Crack growth per cycle |
| K or K_I | Stress intensity factor |
| P_p | Pore pressure |
| S_V | Vertical stress |
| S_h | Minimum horizontal stress |
| S_H | Maximum horizontal stress |
| T_o | Tensile strength |
| Q | Flow rate |
| ΔP_f | Fluid pressure |
| V_{inj} | Fluid volume injected |

1 Introduction

The recent growth in energy technologies like shale gas and geothermal, as well as the management of subsurface gas reservoirs has led to increased human interaction with rocks in the Earth's crust. The key ingredient in the discussion of extraction and storage of energy are subsurface fracture systems, their geometry, stability and nucleus of instability documented in induced seismic events monitored close to the underground facilities. This is because human activity perturbs subsurface stresses by fluid-injection or depletion induced by pore pressure changes, causing fractures to become unstable, to propagate and coalesce. Even though the seismic radiated energy is only a small fraction of the pumped-in hydraulic energy, e.g. in the hydraulic fracture growth process, felt induced seismic events associated with human operations in the subsurface terminated some projects (Giardini 2009). The goal, therefore, is to manage subsurface sites without the occurrence of seismic events of economic concern (Grünthal 2014). At a specific location this task can be fulfilled, only if one is able to detect, image and control fractures for the mechanical and hydraulic integrity of the reservoir under investigation. While many articles exist reporting fluid induced seismicity, very few articles deal with suggestions on how to mitigate and reduce fluid-induced seismicity. The over-arching goal is to reduce the magnitude of the largest events triggered by fluid injection. In particular the intention is to replace the largest magnitude events by a cloud of many smaller magnitude events. In this context, Yoon et al. (2014) demonstrated by hydro-mechanical coupled simulation of a naturally fractured geothermal reservoir with Soultz-sous-Forêt properties that cyclic injection of fluid compared to monotonically increasing the injection rate has the capacity to lower the number of larger magnitude events. The maximum allowable magnitude has to be determined for each site individually through a detailed process of risk assessment (Majer et al., 2012). The maximum allowable magnitude depends on the peak ground velocity at the surface, the local geology, and surface structures. One option is to keep seismicity so low that it is not perceptible by humans on the surface. For this, Westaway and Younger (2014) suggest for the UK that the existing regulatory limits applicable to quarry blasting (i.e. peak ground velocities in the seismic wave field incident on any residential property of 10 mm s⁻¹ during the working day, 2 mm s⁻¹ at night, and 4.5 mm s⁻¹ at other times) could be readily applied to cover such induced seismicity. Another option is to use seismic traffic light systems, which are widely accepted as risk mitigation procedures for hydraulic treatments (Bommer et al. 2015; Maxwell et al. 2015). Many concepts were proposed (e.g. Bachmann et al. 2011; Mena et al. 2013), but only few of them were actually applied in the field (e.g., Bommer et al. 2006; Häring et al. 2008). All traffic light systems have in common that fluid injection is stopped, the treatment pressure is reduced or the well is shut-in or flown back if certain thresholds of seismic magnitudes or other observations are overcome during injection.

According to McGarr et al. (2015), fluid-induced seismicity from human operations results from five different causes (classes of fluid-induced seismicity). Injection activities to be distinguished are (1) disposal of wastewater into deep formations, (2) injection of water or CO₂ into depleted reservoirs for enhanced oil recovery, (3) hydraulic fracturing to enable production of oil and gas from low-permeability rock, (4) injection of CO₂ for

permanent carbon capture and storage, and (5) development of enhanced geothermal systems (EGS). Review articles are available for the different classes of fluid-injection induced seismicity. For example, Suckale (2009) and Davies et al. (2013) reviewed induced seismicity in hydrocarbon fields. Warpinski et al. (2012) elaborated on induced seismicity related to hydraulic fracture operations in shale gas extraction. At European scale, Evans et al. (2012) separated crystalline from sedimentary environments, and reviewed induced seismicity from fluid-injection into geothermal reservoirs and CO₂ storage sites. For the US, Ellsworth (2013) focused on injection-induced earthquakes caused by wastewater disposal. Zang et al. (2014) gave an overview of induced seismicity in geothermal operations with emphasis on EGS, but also in comparison to other classes of fluid-induced seismicity. Rubinstein and Mahani (2015) discussed fluid-induced seismicity related to wastewater injection, hydraulic fracturing and enhanced oil recovery. All reviews above, including the recent one by Foulger et al. (2018), beside from monitoring strategies and traffic light systems do not discuss innovative technologies how to actually reduce fluid-induced seismicity, e.g. by advanced injection schemes. Better knowledge of the stress and pressure conditions at depth; the hydrogeologic framework, including the presence and geometry of faults; and the location and mechanisms of natural seismicity at a few sites will be needed to develop a predictive understanding of the hazard posed by induced earthquakes (Ellsworth 2013). We all are aware that earthquakes can be induced by fluid injection. Industry needs clear requirements under which to operate with current technology, or needs new technologies based on fracture mechanical, hydro-mechanical and seismo-mechanical principles in order to mitigate larger magnitude events.

Class (1) and (4) of fluid-injection induced seismicity involve large net volumes of fluids injected into the crust. Therefore, these long-term operations carry the risk of inducing larger seismic events. Analyzing 187,570 wastewater injection wells in the US, Weingarten et al. (2015) discussed several operational parameters hypothesized to influence the likelihood of an induced seismic event. Among them are the injection rate (Frohlich, 2012; Keranen et al., 2014), the cumulative injection volume (McGarr, 1976, 2014), the wellhead injection pressure (Block et al., 2014) and the proximity of the injection depth to the crystalline basement (Kim, 2013). At the scale of their study, the monthly wellhead pressure, injection depth, and proximity to crystalline basement do not strongly correlate with the induced seismicity observed. Managing injection rates of disposal wells seems to be a useful tool to minimize the likelihood of induced earthquakes. In some areas, however, other factors in addition to the high injection rate must play a significant role. Among these factors, the stress state, the fault size and orientation, the presence of fluid pathways between injection point and fault, and other geological factors warrant further investigation.

In this study, we follow Zang et al. (2014) and differentiate between long-term injection operations (class (1) and (4)), and short-term fluid injection operations (class (2), (3) and (5)). Of the short-term injections, EGS stimulations have in general shown a higher propensity to produce larger induced events (Zang et al. 2014), compared to hydraulic fracturing in oil and gas operations (Warpinski et al. 2012). This statement, however, is invalid when subsurface hidden faults come into play and are interacting with the cloud of induced seismic events resulting from fluid injection. For example, Wilson et al. (2018) suggest a horizontal respect distance of 895 m between horizontal fracking boreholes (drilled parallel to the maximum horizontal stress) and faults optimally oriented for failure. In the subsection that follows, we focus on short-term fluid-injection experiments. We do not know, however, if cyclic injection at longer time scales and different pressure range can be applied to lower seismic hazard also in wastewater disposal scenarios. In section 2, we present the underlying concept of fatigue hydraulic fracturing. Our working hypothesis is that advanced fluid injection schemes like cyclic, progressive and/or pulse fatigue hydraulic fracturing allow for the mitigation of larger seismic events. We see rock fragmentation by hydraulic fatigue as an energy efficient process. This is because laboratory triaxial tests with cyclic pumping indicate a wider fracture process zone (consisting of grain boundary cracks) as compared to a smaller, more localized fracture process zone (consisting of transgranular cracks) generated in conventional hydraulic fracturing with monotonic increase in the injection pressure. In section 3, we report on controlled experiments with advanced fluid-injection schemes at different scales. In section 4, results from laboratory testing on cores and a water injection experiment in an underground research facility are summarized. The impact of fluid flow rate and fluid volume injected on hydraulic fracture growth in naturally fractured granite at depth is discussed together with induced seismic events and radiated seismic energy rate. In section 5, advantages and disadvantages of fatigue hydraulic fracturing applied to geothermal energy applications are discussed in the framework of energy partition (injection efficiency), cost effectiveness, and seismic hazard aspects.

1.1 Short-term fluid-injection experiments

In Figure 1, the maximum observed magnitude of seismic events is plotted versus the volume of fluid injected for different types of fluid-injection experiments (geothermal, wastewater, shale gas, KTB deep well). The upper bound of the maximum magnitude comes from the linear relationship postulated by McGarr (2014) while the

lower bound is obtained from observed values resulting from 30 different fluid-injection experiments in the field, color-coded according to the in-situ stress field at target depth (modified from Zang et al. 2014). From Figure 1 it is evident that long-term injection experiments (e.g., injected volumes $>100,000 \text{ m}^3$) follow the linear upper bound of McGarr (2014) closer than short-term injection experiments. Short-term injection experiment (e.g., days and weeks with injection volumes $< 100,000 \text{ m}^3$) show data points that start to deviate and plot at much lower values than expected from the McGarr boundary, in particular for small fluid volumes injected. For a similar value of fluid volume in short-term EGS stimulation, the observed maximum magnitude in the reservoir ranges between $M_w = -1$ (Fig. 1, #7, Groß-Schönebeck EGS, $13,000 \text{ m}^3$ injected, Zimmermann et al. 2010) and $M_w = 3.4$ (Fig. 1, #2, Basel EGS, $11,570 \text{ m}^3$ injected, Häring et al. 2008). This is a clear indication that for short-term injection experiments (classes (2), (3) and (5)) factors other than the total volume of fluid injected need to be taken into account. Among them, hydraulic parameters (injection rate, wellhead pressure, injectivity) and mechanical reservoir parameters (rock properties, in situ stress at target depth) can be of interest.

Fig. 1 Summary of relationship between maximum observed seismic magnitudes and fluid volume injected in different field experiments. Symbols indicate geothermal, shale gas, wastewater disposal and KTB deep fluid injection experiment. Colour indicates in situ stress regime at target depth (*red* = normal faulting, *purple* = strike slip, *blue* = thrust faulting regime). Upper bound is the linear relationship postulated by McGarr et al. (2014). Lower bound values come from the extended EGS data base published by Zang et al. (2014).

Also, the seismic efficiency (ratio of radiated seismic and pumped-in hydraulic energy) is worth considering when dealing with different reservoir rock in different energy extraction technologies (e.g., gas from shale, heat from granite). A variety of seismic injection efficiencies have been reported for different energy technologies (Maxwell 2013; Zang et al. 2013; Goodfellow et al. 2015; Yoon et al. 2015a). According to this, careful analysis is needed to understand and control short-term injection experiments in the field. The reduction of the total pumped volume or slow injection operations may reduce seismic hazard. However, how the injected volume, the rate of flow and the injection pressure relate to seismic energy release in oil and gas, and in particular to the occurrence of larger seismic events is still a matter of debate (Warpinski 2013; Maxwell et al. 2015). In EGS, a man-made reservoir needs to be created where there is hot rock but insufficient permeability or fluid saturation for geothermal production. The key task here is to create a cubic kilometer scale reservoir and produce energy without adverse environmental effects, such as induced seismicity. In the European Union project GEISER (2010-2013), the major goal was to understand and mitigate induced seismicity in geothermal reservoirs. Results of site-specific geothermal seismicity in comparison to other types of induced seismicity including hydraulic fracturing in shale gas, wastewater disposal and KTB deep fluid injection experiments are published in a Special Issue, GEOTHERMICS October 2014. The next step is to apply so-called soft stimulation techniques developed at borehole scale (EU project DESTRESS, 2017-2020).

After hundreds of thousands of shale-gas fracturing stages conducted to date, there are only a few documented examples of felt seismicity (Maxwell 2009; Davies et al. 2013). These events are related to the reactivation of pre-existing fault zones. Recently, however, more and more studies are published addressing the issue of fault activation by hydraulic fracturing (Clark et al. 2014; Friberg et al. 2014; Bao and Eaton 2016; Wang et al. 2016). In this context, it has to be pointed out that the moment magnitude fluid volume relationship discussed in Figure 1 becomes invalid when the induced seismic cloud (resulting from any energy extraction or wastewater disposal scenario) approaches a tectonic fault or fault system. In this case, the moment magnitude can easily increase by two orders of magnitude (i.e., 1000 times the energy), as documented in Wolhart et al. (2005) and Maxwell et al. (2009). In this case, as suggested by Zang et al. (2014) in the framework of EGS analysis, careful monitoring of subsurface fluid-injection experiments is required with surface and borehole sensors to detect runaway fractures, also along buried faults. This problem, however, is excluded from the analysis of induced seismicity in this article.

As field testing in wellbores is time consuming and costly, we see controlled experiments in underground research facilities as a valuable alternative to seek for optimum energy extraction methods with sophisticated fluid-injection schemes. The optimization process can involve fracture design with reduced seismic radiated energy and/or fracture design with maximum permeability enhancement. For this, radiated seismic energy and pumped-in hydraulic energy needs to be quantified for various advanced fluid-injection schemes applied to different rock types in well-known stress conditions.

2 Concept of fatigue hydraulic fracturing

The concept of Fatigue Hydraulic Fracturing, FHF has been proposed and discussed in geothermal applications (Zang et al. 2013; 2017ab). Since in some articles the basic idea of the FHF concept has been misinterpreted (Zhou et al. 2017), we briefly recapitulate the three steps required to upgrade from mechanical cyclic loading

(mechanical fatigue), over hydraulic cyclic pumping and pulse fracturing to the final product of FHF (hydraulic fatigue).

2.1 Mechanical cyclic loading (mechanical fatigue)

Fatigue is the progressive and localized structural damage that occurs when a material is subjected to cyclic loading (Crane and Furness 1997, their Chapter 9). The two key features of fatigue compared to conventional failure are the following. First, fatigue occurs at a load lower than the required load to produce failure by static loading. Second, fatigue is a violent form of fracture without early warning from material behavior. The micro-mechanism of fatigue is well investigated in metals, but is rudimentarily known in brittle materials like ceramics, concrete and rock. The assessment of fatigue through fracture mechanics is given by the Paris-Erdogan law (Paris and Erdogan 1967)

$$\frac{dc}{dN} = A(\Delta K)^m. \quad (1)$$

This law assumes a simple power law relationship between the crack growth rate, dc/dN , and the range of stress intensity factor, ΔK , during the mechanical loading process with N cycles and constants A and m . Some results of laboratory experiments with mechanical cyclic loading are presented in Haimson and Kim (1991), Erarslan and Williams (2012), and Ghamgosar and Erarslan (2016). One end-member test with very tiny load step cycles is presented by Lockner et al. (1991) to control rupture speed of laboratory fracture experiments. The technique is based on a sophisticated acoustic emission rate control system which is coupled to the servo-controlled mechanical loading frame used in compression experiments. Such a setup has been used by Zang et al. (2000) to determine the acoustic and optical width of the fracture process zone, FPZ from propagating single shear ruptures in granite. Monotonic and cyclic mechanical loading produce different size process zones. This has been documented for different rock types, e.g. granites and sandstones (Zang et al. 2002) and tuff and monzonite (Ghamgosar and Erarslan 2016). Slow fractures generated by cyclic mechanical loading produce smaller FPZ when compared to fast fractures generated with displacement-controlled, monotonic mechanical loading. A recent review paper on mechanical fatigue has been published by Cerfontaine and Collin (2017).

2.2 Hydraulic cyclic pumping (hydraulic fatigue)

As in the mechanical cyclic loading case, in the cyclic pumping case the injection pressure is lowered frequently in order to allow stress relaxation at the fracture tip (Zang et al. 2013). However, the fatigue process during cyclic mechanical loading (Erarslan and Williams 2012), can be very different from fatigue hydraulic fracturing where a high-pressurized fluid is operating at the fracture tip (Zang et al. 2017b). The reason for this is that fracture fluids affect the fracture strength through a direct pressure effect (cycles of high fluid pressure) and through a chemical interaction with the matrix of silicate rocks (subcritical crack growth, Atkinson 1984). Also, the fracturing fluid plays a role (Wang et al. 2018). The direct pressure effect can be taken into account by using an effective stress law for hydraulic fracture growth (see e.g. Patel et al. 2017):

$$FBP = 3Sh - SH + To - p(t). \quad (2)$$

The fracture breakdown pressure, FBP, in hydraulic fracturing is computed from the total stress in the rock mass (horizontal minimum (Sh) and maximum stress (SH)), the hydraulic tensile strength, To and the fluid pressure rate changes, $p(t)$, resulting from the fluid-injection scheme applied. Equation (2) illustrates that a fracture in hard rock is initiated at a given stress state and tensile strength at first breakdown pressure FBP under the assumption that the pore pressure in the rock mass is zero, $p(t)=0$. A fracture process zone FPZ with meso- and micro-fractures is generated at the tip of the breakdown fracture. A cyclic hydraulic fracturing, CHF implies the high fracture pressure is brought down to zero and rests at zero pressure for a given time. The following cycle starts with monotonic increasing pressure till the fracture reopens and propagates at the reopening pressure, lower than FBP. During pressurization, the reopening pressure enters the meso- and micro-fractures in the FPZ with the amount $p(t)$ and thereby lowers the rock mass strength. A continuous CHF will further propagate the fracture at constant injection pressure (cf. Figure 2).

The second process affecting fracture strength is caused by the disruption of Si-O bands in silicate rocks by reaction with water. Chemical assisted crack growth is seen as the primary mechanism for stress corrosion by providing a mechanism for crack growth below the critical stress intensity factor. The subcritical crack growth rate, dc/dt is related to the stress intensity factor in tension (mode I), K_I by

$$\frac{dc}{dt} = A(K_I)^n, \quad (3)$$

where A and n are constants. For example, the power exponent n is on the order of 15 to 40 for granitic rocks.

The fracture mechanism involved in cyclic pumping of high pressurized fluid is known as the Kiel process (Kiel 1977). During cyclic pumping, dendritic (branching) fractures are formed in contrast to hydraulic fracture growth with monotonic pumping. Examples of laboratory experiments with cyclic pumping of fluids into small scale boreholes are Zhuang et al. (2016), Patel et al. (2016), Zhou et al. (2017) and Zhuang et al. (2017). While Zhuang et al. (2016, 2017) tested fluid injection into Pocheon granites cores from Korea (diameter 50 mm, length 100 mm) and analyzed the resulting fracture pattern by X-ray CT, Patel et al. (2016) fluid pressurized Tennessee sandstone cores (diameter 102 mm, length 140 mm) with acoustic emission measurements and electron microscopy fracture damage inspection, and Zhou et al. (2017) used larger scale mortar blocks (300 x 300 x 600 mm) with visual hydraulic fracture inspection with colored injection fluids. In all studies, there is a tendency of lower FBP and a more complex fracture pattern when monotonic pumping is replaced by CHF.

2.3 Progressive cyclic and pulse fracturing (fatigue hydraulic fracturing)

The concept of fatigue hydraulic fracturing is based on a double optimized process (Zang et al. 2017b). First, the cyclic pumping scheme is replaced by cyclic injection with progressively increasing target pressure. Second, in phases of pressurization an overriding dynamic pressure pulse (frequency 5 to 20 Hz) is generated with a second pump. This concept is tested in hard rock with two different hydraulic fracturing companies, and two different pump systems (Zang et al. 2017a). To our knowledge such an advanced fluid-injection scheme for FHF purpose has not been proposed nor previously tested. Historically, cyclic pumping was applied in the stimulation of EGS (Zimmermann et al. 2010). In the concept of “relax a frac” for shale gas extraction purposes, a part of the stimulation treatment was pumped, followed by an extended shutdown to relax the formation (Indamdar et al. 2010). Pure pulse hydraulic fracturing was proposed as tailored-pulse loading by Swift and Kusubov (1982), for fracturing of shale gas (Safari et al. 2015), for testing hydraulic fracturing methods in combination with pulse testing for different rock engineering applications (Jirakova et al. 2015), and for improving drainage of coalbed methane (Xu et al. 2017).

The main goal of FHF is to drive hydraulic fractures in a more controlled way, specifically with minimum seismic radiated energy and maximum permeability enhancement. For this, the FHF treatment is a combination of modified cyclic hydraulic fracturing (CHF) and pulse hydraulic fracturing (PHF). First ingredient in the fatigue treatment is the frequent lowering of the injection pressure. In contrast to the cyclic injection scheme proposed by Kiel (1977), in the fatigue treatment frequent phases of pressurization and depressurization are used while the target pressure is increased progressively (Figure 2).

Fig. 2 Scheme of pumping used in the FHF treatment. (a) Pressure, flow chart of test with four cycles and increasing target pressure, and (b) detail of the progressive cycle 3 at breakdown. The dynamic pulsing (here 5 Hz) applied during the pressurization levels is to disintegrate the rock and remove weak material from fracture faces acting as natural proppants to change the stress field in subsequent cycles of pressurization and depressurization.

This allows the formation of fracture with less fluid pressure compared to the case with continuous fluid injection. For this, smaller pumps can be used which makes the treatment safer. The second ingredient in the fatigue treatment is the overriding dynamic pressure pulse (generated by a separate pump system) which comes on top of the progressively increasing target pressure levels. High frequency water pulses aim to disintegrate and to remove weak material from the faces of the fracture by hydraulic fatigue and locally decrease the strength of rock by generating an enlarged fracture damage zone (Figure 3). This FHF pumping scheme developed at mine scale is designed for (1) the breaking of naturally fractured hard rock with lower fluid pressure, (2) the generation of a more complex fracture pattern for permeability enhancement, and (3) the replacement of larger seismic events by a cloud of smaller event resulting from an optimized rock fragmentation process as compared to conventional hydraulic fracturing with monotonic, continuous fluid injection.

Fig. 3 Synoptic view of the fracture process zone resulting from (a) conventional hydraulic fracturing with monotonic increase of injection pressure, and (b) fatigue hydraulic fracturing with frequent phases of depressurization and oscillating pulses during pressurization phases. In (b) rock chips removed from fracture faces through high frequency vibrations (secondary pump) and washed out to the fracture tip allow a change in the local stress field in depressurization phases of the FHF treatment. A larger fracture process zone is created (b), compared to the case with continuous fluid injection in conventional hydraulic fracturing (a).

3 Controlled experiments with advanced fluid-injection schemes

Strictly speaking, three types of fluid-injection experiments can be distinguished. The first type is related to direct injection of fluids into a well-characterized fault at depth with simultaneous monitoring of the seismic and aseismic response of the host rock (e.g., Guglielmi et al. 2015). The second type of controlled underground experiments is related to determination of the seismic efficiency of hydraulic fracture growth (remote from any fault system) together with rock fracability and permeability by applying advanced fluid injection schemes with multiple rates of flow and two or more pumping systems, specifically for developing an optimum heat exchanger area in granitic rock at depth (Zang et al. 2017a). The third option is a combination of the two previous types of experiments, and includes propagating an hydraulic fracture at some distance from a fault into the fault zone. So far, this latter scenario has only been investigated in detail by numerical analysis (Rutqvist et al. 2013, Yoon et al. 2015b, Rutqvist et al. 2015), but seems to be of relevance in field injection experiments like Paradox Valley, Colorado (Yeck et al. 2015) or Prague, Oklahoma (McMahon et al. 2017). In the following, we describe a type two experiment where hydraulic fractures were propagated in multiple stages with a progressive cyclic water-injection scheme and/or a pulse dynamic water-injection at depth in Äspö Hard Rock Laboratory, Sweden. In the subsection that follows, we start referring to small scale laboratory fluid injection experiments on granite cores with subsequent fracture pattern analysis through X-ray computer tomography.

3.1 Small scale laboratory experiments on granite cores (injection borehole diameter 8 mm)

Laboratory experiments using granite core samples were conducted at the Korea Institute of Civil Engineering and Building Technology (KICT). The cores were extracted from Pocheon, Korea. The granite cylindrical specimens have a diameter of 50 mm, and a height of 100 mm. To simulate a borehole, a perforation of 8 mm in diameter passes through the center of the cylindrical cross section and along the entire height. Pocheon granite specimens were prepared considering the planes of weakness commonly known as rift, grain and hardway (Nichols 1975). To test these specimens, an hydraulic fracturing test equipment is developed and its main components are shown in Figure 4. The equipment is able to provide maximum vertical and confining pressures of 50 MPa and 20 MPa through a servo-hydraulic loading system, respectively. An additional line supplies the injection fluid at the bottom of the specimen with a maximum injection pressure capacity of 35 MPa (Fig. 4c). To prevent fluid leakage, nozzle plates with o-rings are attached to the top and bottom of the specimen. Then, the specimen sets on a pedestal that supplies the injection fluid and a plastic membrane is installed to protect the specimen from the oil that provides confining pressure. Fluid injection can be conducted under injection rate or pressurization rate control. Pressure evolution is recorded during each test. Once the hydraulic test is over, the specimen is taken for X-ray CT scanning to observe and measure fracture geometries (Fig 4d). Acoustic monitoring is carried out with an array of 8 Nano sensors attached to the specimen surface with a coupling agent to improve contact. Test described are conducted without confining pressure. A new set of triaxial tests with cyclic pumping has been conducted but is not evaluated in detail for this study.

Fig. 4 Laboratory equipment for hydraulic fracturing at KICT: (a) Control unit, (b) hydraulic pump, (c) tri-axial cell, and (d) interior view of the working table of the industrial X-ray CT scanning used.

3.2 Intermediate scale experiments in granitic rock (injection borehole diameter 102 mm)

The Äspö Hard Rock Laboratory (HRL) is located in the southeastern part of Sweden about 30 km north of the city of Oskarshamn. It has been selected to fix some variables to perform controlled fluid injection experiments. In the first place, the stress state at 410 meter depth is fixed, and well known from hydraulic fracturing (Klee and Rummel 2002) and overcoring stress measurements (Ask 2006). Second, the granitic rock type is fixed, and relevant for geothermal reservoir development. Äspö granodiorite and fine-grained granite are well characterized, both mechanically and hydraulically. Third, the total volume of fluid injected is limited to 30 liters maximum. Therefore, we focused on varying the injection style while controlling the hydraulic energy and monitoring the seismic energy in naturally fractured granitic rock mass with size of about 30 x 30 x 30 m, see Figure 5. Selection of hydraulic test intervals is based on the inspection of diamond drill cores continuously cored and on the inspection of the borehole by image tools (Zang et al. 2017a). Six sections free of visible fractures were identified for hydraulic testing. Three different water-injection schemes were applied (continuous, progressive and/or pulse injection).

Conventional hydraulic fracturing HF with continuous fluid injection follow the ISRM suggested method for hydraulic fracturing stress measurements (Haimson and Cornet 2003). The typical test starts with the initiation of the packer system to seal the interval, followed by a rapid pressurization with water to test the system for potential leakage (pulse integrity test). During the subsequent main test phase a constant injection rate is applied. Pressure increases until it reaches the FBP, followed by a decline to a stable pressure level called the fracture propagation pressure (FPP). After stable pressure conditions are reached, the well is shut-in and the pressure

drops rapidly to the instantaneous shut-in pressure (ISIP) followed by a decline curve. The ISIP is assumed to be equivalent to the minimum principal stress. Finally, the interval pressure is released and the fluid volume is recovered. The test procedure is repeated several times to obtain the fracture reopening pressure (RFP) at each test cycle. The tensile strength of rock, T_0 , is calculated from FBP-RFP. It is assumed that the fracture has been closed completely in between the cycles.

The test procedure for the progressive water injection consists of a modified pressure scheme. First the pressure is increased to 20 % of FBP obtained from the conventional test in the same formation. Then, a shut-in for several minutes follows with subsequent pressure release (depressurization phase). Thereafter, the pressure is increased by a level approximately 10 % above the previous pressure level following the same scheme. After shut-in another depressurization phase follows. The pressurization and depressurization sequences are repeated until a pressure drop indicates rock failure. This treatment is best described as a cyclic hydraulic pressure scheme with progressively increasing target pressure. The subsequent re-fracturing stages follow the same scheme like the repetitions in the conventional test procedure. Conventional and progressive treatments differ only for pressures below the FBP, i.e. single-flow rate versus multiple-flow rate fracture breakdown tests.

The fatigue hydraulic fracturing (FHF) test procedure is a combination of the progressive injection test and a pulse hydraulic fracturing (PHF) test. The hydraulic equipment for the pulse dynamic test consists of a hydraulic pump to maintain linear and dynamic pressure levels (pressurization bands) together with a second hydraulic pressure pump to drive the dynamic pulse tool with adjustable amplitude and frequency (5 - 6 Hz in experiment HF5, see Fig. 2). Both pressure signals are combined to result in dynamic pressure pulses on different predefined hydraulic pressure levels based on the FBP of conventional tests carried out previously. The FHF test is best described as a test with cyclic increasing target pressure and additional high frequency pressure oscillations in pressurization phases with step-wise increasing target pressure. This test procedure is frequently interrupted by depressurization phases where crack tip stresses are released.

Fig. 5 Hydraulic fracture design and high-frequency sensor monitoring network at 410 m depth in Äspö HRL. (a) View of the horizontal hydraulic fracturing borehole F1 drilled in the orientation of S_h . Colour coded disks along F1 indicate locations of mid injection intervals. Monitoring boreholes left and right of the fracturing borehole F1 are equipped with AE sensors. Short boreholes in tunnel roofs are equipped with both, AE sensors and accelerometers. (b) Installing a chain of AE sensors in one of the inclined monitoring boreholes in tunnel TASN.

The in-situ testing of different injection schemes with monitoring associated seismic and electro-magnetic signals is conducted in the horizontal borehole F1, 102 mm in diameter and 28 m long, drilled from tunnel TASN in the direction of minimum horizontal stress (Figure 5a). The fracturing borehole is indicated by colored disks representing the injection intervals and the proposed propagation planes of radial hydraulic fractures following the on-site in situ stress conditions ($S_V = S_H > S_h$). The high frequency seismic network used consists of eleven acoustic emission (AE) sensors (Fig. 5a, yellow marker, frequency 1-100 kHz) and four accelerometers (Fig. 5a, green marker, frequency below 25 kHz). AE sensors are implemented in three monitoring boreholes located left and right of the hydraulic testing borehole (Fig. 5a, grey lines with yellow markers). In Figure 5b, the implementation of a chain of AE sensors is shown in one of the inclined monitoring borehole at the end of tunnel TASN. The remaining AE sensors and accelerometers are implemented in short boreholes in the roof of the surrounding tunnels. This monitoring design allows tracking the radial fractures from the nucleation point (injection interval in the testing borehole) towards the arresting point close to the monitoring boreholes equipped with high frequency sensors. This is because the hydraulic fracture use to open perpendicular to the minimum principal stress S_h (perpendicular to the axis of the injection borehole), and rapidly grows in the plane containing the intermediate S_H and maximum principal stress S_V (parallel to the orientation of tunnel TASN).

A triggered and continuous recording system was in operation at 1 MHz sampling rate. This allowed for real-time tracking of the hydraulic fracture growth process (Kwiatek et al. 2017ab), and post-processing of full waveforms (Lopez Comino et al. 2017ab) for source analysis. From a seismological point of view, full waveforms recorded during injection tests have excellent data quality for further processing, which includes hypocenter locations, relocations, and in depth investigation of fracture source, growth and coalescence mechanism.

4 Results

In this section, results from testing the FHF concept at two different scales are presented. In section 4.1, results from cyclic fluid-injection experiments at laboratory scale are expanded. In section 4.2, the main findings from the underground tests in Äspö HRL are described.

4.1 Laboratory results on granite cores

Laboratory experiments on granite core samples under monotonic and cyclic injection indicate a reduction in breakdown pressure and acoustic events amplitude. Figure 6 shows the results of FBP and maximum amplitude from the two sets of tests conducted under monotonic and CHF respectively. Five specimens were tested under monotonic water injection (Fig. 6, circles) at a rate of 50 mm³/s. The average breakdown pressure is found to be 7.18 MPa. For the second set of tests, 20 specimens are tested under cyclic injection (Fig. 6, triangles). In each test, a maximum injection pressure lower than the monotonic average is set as an upper limit, and cyclic injection is continued until specimen failure is achieved. Maximum pressures range from 77% to 101% of the average monotonic FBP. The average FBP for cyclic injection is 6.52 MPa, although the specimens fail after different number of cycles. The acoustic events have an average maximum amplitude of 93.8 dB for monotonic injection and 67.8 dB for cyclic injection, respectively. On average, the FBP is reduced by ca. 10%, and the average maximum acoustic emission event magnitude is reduced by 26 dB when replacing monotonic by CHF using the same experimental setup and sample geometry (Fig. 6, dashed lines).

Fig. 6 Breakdown pressure and maximum event amplitude during five monotonic and twenty cyclic injection tests of Pocheon granite core samples. Dashed lines indicate average values of monotonic and cyclic tests, respectively.

To compare fracture patterns from monotonic and cyclic injection treatment, 3D X-ray computed tomography images are used after each test. Figure 7 shows the apparent difference in geometry of induced fractures for cores undergoing different numbers of hydraulic cycles. In Figure 7a, representative section CT images are selected for three different cases (monotonic, 473 cycles, 839 cycles). To analyse the hydraulic fracture path in a more quantitative way, fracture only images are extracted from the CT images (Fig. 7b). It is observed that induced fractures from monotonic injection have larger apertures than cyclic fractures. Regarding the complexity of fracture pattern, we computed the tortuosity (length of fracture path divided by shortest distance between fracture tips). Tortuosity values are 1.04, 1.05 and 1.09 for the three cases displayed in Figure 7b (from left to right), although a very limited domain is considered for this measurement. A more complex fracture pattern is also supported by the AE monitoring results. Significantly more AE events are detected in the two cyclic injection cases (346 AE events during the test with 473 cycles, 862 AE events during the test with 839 cycles) compared to monotonic injection case (221 AE), when counting AE numbers from the fracture breakdown pressure to one minute after.

Fig. 7 Visualized fracture pattern of granite cores after monotonic and cyclic injection. (a) X-ray CT images, and (b) fracture only images.

4.2 Underground test results in granitic rock mass

In this subsection, the seismic footprint of decameter scale hydraulic fractures generated with different water-injection schemes (4.2.1), their permeability enhancement process (4.2.2), and the resulting fracture pattern from impression packer results are summarized (4.2.3).

4.2.1 Seismic footprint of hydraulic fractures

The seismic response of the high-frequency sensor network from six hydraulic tests in the horizontal borehole at 410 m depth is discussed in this subsection. In Figure 8, hydraulic test parameters like FBP, RFP, flow rate and injected volume are compared with the total number of acoustic emission events localized (color bars) for different rock types and injection schemes. In Figure 9, the localized acoustic emission events are plotted in space together with tunnel geometry and fracturing borehole, F1 and three monitoring boreholes (Kwiatek et al. 2017b). In the deeper section of the horizontal borehole, F1 three hydraulic tests are carried out in Ävrö granodiorite, two conventional continuous injection tests and one progressive cyclic injection test. Compared to the conventional tests (HF1, HF2), the acoustic emission activity in the progressive test (HF3) started at a later stage of the treatment, and the total number of seismic events was less. Experiment HF3 reveals a fracture breakdown pressure of approximately 9.2 MPa. A conventional test with continuous water injection in the same rock type (HF2), the FBP observed was 15% higher compared to the cyclic progressive test. The two tests in diorite gabbro generated only one single AE event indicating that this rock type is less seismogenic compared to the first rock type tested when monitored with the same trigger level at all sensors. In experiment HF5, the progressive pulse testing was applied mimicking the FHF treatment with the dual pump system (see Fig. 2), which resulted in a lower FBP (9.0 MPa) compared to the conventional test in the same rock HF4 (FBP=10.6 MPa), see Figure 8. In the fine-grained granite close to the tunnel wall (HF6) seismic activity is observed in all

fracturing stages. In contrast to other tests, in the granite the maximum number of seismic events occurred during early stages of the hydraulic fracturing and re-fracturing experiment.

Fig. 8 Number of localized seismic events is shown per fracturing stage for six hydraulic tests in horizontal borehole F1 at 410 m depth in Äspö HRL. Seismicity associated with hydraulic fracture initiation and propagation is sensitive to rock type, fracturing stage and the fluid-injection scheme used. In each experiment, the fracture breakdown pressure, the fracture reopening pressure, the flow rate range, and total volume of water injected is listed right below the experiments identification number (HF1-HF6). The first test, HF1 starts in the deeper part of the 28 m long, horizontal borehole (25 m), and the last test HF6, is operated about 5 m from the onset of F1 at the tunnel wall.

Figure 9 shows the relocated AE hypocenters from the in-situ triggered recordings (Kwiatek et al. 2017b). Color coding of fractures is the same as in Figure 8. The 197 AE hypocenter locations are viewed in the direction of S_H , i.e. perpendicular to the horizontal hydraulic testing borehole (Fig. 9, grey line with color disks). While hydraulic fractures HF1, HF2 and HF6 form a single fracture plane documented by AE hypocenters, the progressive water injection test produces a cloud of AE hypocenters not related to a single, planar structure. No AE signals are located during cyclic progressive pulse testing (HF5).

Fig. 9 Locations of 197 AE hypocenters (colour spheres) from six hydraulic testing intervals (colour disks) viewed in the direction of maximum horizontal stress at 410 m depth in Äspö HRL (Kwiatek et al. 2017b, snapshot of movie). In the conventional tests with green (HF1), blue (HF2) and yellow injection intervals (HF6) the AE hypocenters form a planar structure (colour dots). In experiment HF3 with progressive CHF, a cloud of AE is observed. Length of horizontal testing borehole F1 with colour disks is 28 m. AE magnitude is indicated by the size of the color spheres.

4.2.2 Permeability enhancement process

In Figure 10, the permeability enhancement process of conventional hydraulic fracturing (Fig. 10a, HF2) and cyclic, progressive hydraulic fracturing (Fig. 10b, HF3) is compared in the same rock type (Ävrö granodiorite) at injection intervals 3.5 meters apart. In the conventional test HF2, AE occur in all fracturing stages (except Refrac 2). The permeability is estimated from the hydraulic pressure decay curves (see Zimmermann et al., this issue). The initial permeability of rock can be estimated from the first data point in the fatigue test, e.g. 0.1 mD (Fig. 10b, upper panel). In this test, the sustainable increase in permeability is 1.2 mD after the initial fracturing, and 3.8 mD after the last Refrac stage. In the same period of time, 8 AE are registered before the FBP, and 102 AE at the end of the experiment. In the cyclic progressive test HF3, seismicity is observed in the last two re-fracturing stages only (Fig. 10b). The amplitudes of AE in cyclic injection are systematically lower when compared to monotonic injection. The permeability increases monotonically in cyclic treatment from 0.5 mD before FBP to 2 mD after the last re-fracturing cycle (Refrac4). For convenience, the relative permeability (normalized to the initial permeability value) is also plotted in Figure 10 (upper panel, right ordinate). This demonstrates that the injection style has a strong influence on both, the total number of seismic events (conventional 102, cyclic progressive 16), and the relative value of permeability enhancement (conventional 5 times, cyclic progressive 10 times).

Fig. 10 Permeability enhancement process (upper panel) and seismic activity according to injection style flow rate and pressure chart (lower panel) . (a) Experiment HF2 with continuous water injection, and (b) experiment HF3 with cyclic, progressive water injection. Absolute permeability is indicated on left ordinate, and relative permeability is indicated on right ordinate of upper panel view graphs.

4.2.3 Hydraulic fracture pattern

When comparing the orientation of hydraulic fractures in Ävrö granodiorite we find from impression packer results a single fracture plane in conventional testing (HF1 and HF2), and we find two fracture planes in the progressive test HF3 (Zang et al. 2017a). In HF3, AE hypocenters indicate a more complex fracture pattern due to a cloud rather than planar structure. In general, hydraulic fractures are oriented with respect to the measured in situ stress field at 410 m depth (Ask 2006). At present, no more information is available on the complexity of fractures at mine scale.

5 Discussion

The mechanism operating in-situ during fatigue hydraulic fracturing is seen as follows. The cyclic progressive treatment guarantees that the optimum stress state with minimum FBP of the formation (Fig. 2, pressurization phase 3) is found. The dynamic water pulse added to the progressive pressure levels (Fig. 2, pressurization phases 1-4) disintegrates the rock in a different way (Fig. 3b) Permeability increase can result from rock chips moved with the fluid to the fracture tip causing local stress redistributions favoring arrest and branching of fractures (Kiel 1977). In contrast to the Kiel process, where rock chips are produced in the shut-in phase of the

first depressurization level, in fatigue hydraulic fracturing the rock is disintegrated more efficiently by using a second, high-frequency pump system operating during pressurization levels. In line with the Kiel process, the rock mass strength may be decreased by the formation of an enlarged hydraulic damage zone (Fig. 3b, kidney-shaped FPZ). At the moment, we have no clear evidence for the rock disintegration process. However, smaller event magnitudes during cyclic injection support a different process when compared to monotonic injection (Fig. 6). Also, cyclic triaxial fluid injection tests on Pocheon granite indicate different fracture types (grain boundary) from those found in monotonic triaxial injection tests (transgranular). This observation is in line with cyclic triaxial testing of Tennessee sandstone reported by Patel et al. (2017).

From uniaxial testing on Pocheon granite with an injection borehole diameter of 8 mm in this study, the fracture breakdown pressure is decreased by 10% when replacing monotonic (FBP= 7.2 MPa) by CHF (FBP= 6.2 MPa). Also, the amplitude of induced acoustic emissions is reduced by 26 dB on average when replacing monotonic injection (94 dB) by CHF (68 dB). Through-going fractures were observed by X-ray CT in monotonic injection, and arresting and branching fractures are observed in the CHF case. Note that in recent triaxial tests on the same granite, more grain boundary cracks are found in cyclic injection as compared to monotonic injection (Zhuang et al. 2018 submitted).

In triaxial testing of Tennessee sandstone cores, Patel et al. (2017) found that the FBP is decreased by 16% using CHF instead of conventional hydraulic fracturing. This applies to dry Tennessee sandstone. CHF in saturated Tennessee sandstone, however, does not have any effect on the FBP. One reason for this may be the initial porosity of the sandstone (6%) as compared to the porosity of tight granitic rock (below 1%) investigated in this study. Second, Patel et al (2017) report an increase in the total number of acoustic events and pre-breakdown acoustic events in CHF. However, no amplitude classification of acoustic emissions is carried out. Our study suggests that the overall average of maximum magnitudes decreases when applying CHF. Third, Patel et al. (2017) report fracture permeability of Tennessee sandstone which increases by a factor of three to ten when replacing conventional by CHF in a confined test. The increase in AE number and fracture permeability in CHF suggests an enlargement of the FPZ which is confirmed by electron microscope analysis post mortem. In dry Tennessee sandstone, the analysis shows damage around hydraulic fracture generated by CHF to be twice that generated by conventional injection. This finding supports the idea that confined CHF generates a larger FPZ as compared to conventional fracturing in line with the conceptual FPZ in Figure 3.

At mine scale and decameter size hydraulic fractures, FBP in Ävrö granodiorite was lowered by 15% when using neighboring test intervals 3.5 m apart, and replacing monotonic (FBP= 10.9 MPa) by cyclic, progressive water injection (FBP=9.2 MPa). The total number of AE located was reduced from 102 events (HF2, monotonic injection) to 16 AE events (HF3, cyclic progressive injection). The combination of CHF and PHF (HF5) resulted in zero AE but in a different rock type. The HF5 test resulted in the largest permeabilities of 2.3 mD after the main fracturing stage, and 26 mD and 17 mD after the 2nd and 3rd refrac stage, respectively (Zimmermann et al., this issue). Compared to the initial value of permeability in the conventional hydraulic fracturing test, the permeability increases by 3 mD compared to 2 mD in the cyclic progressive injection case. The relative permeability increase during progressive cyclic test HF3 was 10 as compared to 5 in the conventional HF2 test. In addition, the fracture from impression packer indicates a single fracture plane in conventional tests (HF1, HF2), and a double fracture plane in cyclic progressive testing in the same rock type (HF3). Our results do not support the idea that hydraulic fracture growth is a purely aseismic process. It is a matter of sensors, or combination of sensors (piezo-ceramic versus borehole geophones), that determines if induced seismicity from a propagated hydraulic fracture can be detected or not, see Gischig et al. (2017) and Zang et al. (2017a). We see acoustic emission events originating from process zone related micro-shears (cm to dm-scale) in Ävrö granodiorite (Fig. 3) while we agree with Warpinski et al. (2012) that the amount of energy radiated as elastic waves is only a small fraction of the injection energy of the pump. This result is also supported by tilt measurements of six hydraulic fractures in Äspö Hard Rock Laboratory using broadband seismometers placed in the near-field of the fracture experiments (within 10 m distance from hydraulic fracture faces, Zang et al. 2017a). Gischig et al. (2017) also computed fracture source dimensions of 0.08 m to 0.56 m in Grimsel granodiorite using an analogue combination of sensors as used in Zang et al. (2017a).

The ratio of seismic energy to injection energy is referred to as the seismic injection efficiency (Maxwell et al. 2008). In Figure 11, we compare computed seismic injection efficiency for granitic rocks tested at two different scales: Pocheon granite in the laboratory and Ävrö granodiorite tested in Äspö HRL at 410 m depth. For this, the hydraulic energy of the injection experiments is calculated following Goodfellow et al. (2015, their Eq. (3)) by multiplying the injection pressure and corresponding flow rate with integrating over the duration time of the injection interval. The seismic radiated energy is calculated following Goodfellow et al. (2015, their Eq. (5)). Laboratory acoustic emission magnitudes are computed from Khazaei et al. (2015, their Eq. (2)). The seismic moment magnitude of acoustic emissions registered in Äspö HRL are computed using data from hammer hit calibrations performed in the tunnel surrounding the stimulation site since these signals have been successfully recorded on accelerometers and AE sensors (Kwiatk et al. 2017b). At both scales, the seismic radiated energy is

computed as cumulative value of all events occurring in each test sequence including pre-FBP cyclic injection events and post-FBP events during refrac cycles.

In Figure 11, the seismic injection efficiency is plotted versus the cumulative hydraulic energy pumped into the system for three hydraulic fracturing test in Ävros granodiorite (Fig. 11, *diamonds*, mine-scale, fracture extension 5 m to 12 m) and 20 unconfined hydraulic fracturing test on Pocheon granite core specimens (Fig. 11, *circles*, laboratory scale, crack extension 0.05 m to 0.1 m). In contrast to seismic efficiency data published previously (Maxwell 2013; Zang et al. 2013; Goodfellow et al. 2015), in Figure 11 the number of hydraulic fatigue cycles used is color-coded. Open symbols represent the conventional hydraulic fracturing test with continuous fluid injection. Colored symbols indicate CHF tests with increasing number of fatigue cycles (*black* color= 1 injection cycle, *violet* = 10 cycles, *green* = 100 cycles, and *yellow* = 1000 cycles).

Fig. 11 Seismic injection efficiency plotted against hydraulic energy from laboratory and mine-scale fluid injection experiments. *Circles* refer to laboratory core testing (injection borehole diameter 8 mm) and *diamonds* refer to Äspö HRL underground testing at 410 m depth (injection borehole diameter 102 mm). The number of fatigue hydraulic fracturing cycles is indicated by colour, and ranges from 1 to 839 cycles. For reference, conventional tests with continuous fluid-injection are indicated by open symbols.

In line with the fluid volume pumped into the system and the size of hydraulic fractures generated, the hydraulic energy calculated for the conventional test is about 5 J for laboratory testing (Fig. 11, *open circles*), and on the order of 20 kJ for the underground field test (Fig. 11, *open diamonds*). The corresponding seismic injection efficiency values are 10^{-10} and 10^{-5} for laboratory and underground testing, respectively. Laboratory data with a broad range of injections cycles tested (Fig. 11, *color circles*), indicate that seismic efficiency decreases by five orders of magnitude (Fig. 11, from 10^{-10} to 10^{-15}) when increasing the number of fatigue cycles by about three orders of magnitude (Fig. 11, from 1 to 839 injection cycles). Note that in confined tests, these numbers can change. The absolute values of laboratory seismic radiated energy range between 10^{-9} J and 10^{-12} J while the hydraulic energy pumped into the cores is increasing monotonically from 10 J at one cycle to about 1 kJ at 839 cycles. On the other hand, the hydraulic energy in the underground test does not vary significantly because the total volume of fluid injected is limited to 30 liter and number of fatigue cycles is limited to five (Fig. 11, *dark blue diamond*). In tendency, however, the underground cyclic test shows the same tendency of lower seismic efficiency with increasing number of fatigue cycles as it is found from the laboratory data. The comparison between the cycled and monotonic experiments in the mine is difficult due to the order of magnitude difference in the permeability and in the extent of the fracture process zone. This implies a larger off-fracture volume of rock that is stressed. We admit that this is one of the vagaries of the underground experiment.

At laboratory scale, more work is needed to determine seismic radiated and hydraulic energy as a function of hydraulic fatigue cycles, also in triaxial or true-triaxial testing. Future underground injection experiments should include a test program with increasing number of fluid-injection cycles, e.g. from 10 to 100, and also to vary the frequency of the secondary pump to control the hydraulic fatigue process. The combined interpretation of laboratory and mine-scale tests in the same rock type is seen valuable to identify the mechanism operating in situ when hydraulic fracture faces are periodically pressurized to optimize the fracture growth and the permeability enhancement process.

A full-scale borehole field test requires a careful treatment design. Yoon et al. (2015c) discuss the following operational parameters relevant in FHF testing: Cyclic injection rate, interval injection rate, injection duration, interval duration, rate increment, number of cycles, and interval duration between stages. Recently, a soft stimulation concept is developed for well scale testing. It includes cyclic injection design at three different length scales (days, hours and minutes), avoiding shutting-in the well, limiting maximum pressures to values slightly above the fracture opening pressure, and slowly reducing pressures below the fracture opening pressure during the nights and after the treatment. The treatment design and the adapted traffic light system are presented in Hofmann et al. (2017).

The concept of fatigue hydraulic fracturing is still in the stage of development requiring more fundamental research at various scales and in-situ validation. Based on the abundance of experimental data investigating the effect of cyclic injection on breakdown pressure it can be considered as proven fact that cyclic injection lowers the breakdown pressure. This reduction is on the order of 10 to 20%. A reduction in breakdown pressure has the benefit to use smaller pumps which makes the treatment safer. On the other hand, the reduced pressures may also lower the seismic risk. The concept is currently focused on reducing the magnitude of induced seismicity in crystalline rock formation because of its critical importance for public acceptance especially for deep geothermal energy. Cyclic injection systematically seems to reduce the magnitude of the largest induced seismic event. This was observed at different scales and in experiments where a direct comparison between monotonic and cyclic injection was possible. However, there is optimization potential in finding injection parameters that minimize the maximum seismic magnitude. The total number of fluid-induced seismic events is not consistent, and certainly depends on rock type, stress heterogeneity, and injection scheme. In all experiments it has been demonstrated that cyclic injection consistently increases the hydraulic performance of the system. From underground testing a

cyclic progressive injection scheme in combination with pulse fracturing seems promising. On the other hand, the cyclic opening and closing of the stimulated fractures may have the potential to damage the fractures and reduce its permeability. This effect would likely be more pronounced for soft as compared for hard crystalline rock. Experiments presented by Vogler et al. (2016) on twelve granodiorite samples containing a single fracture from Grimsel Test Site, Switzerland need to be performed at mine scale to evaluate the permeability change and its mechanisms. Asperity breakage during loading cycles needs to be quantified with the observed hysteresis in joint closure curves (Bandis et al. 1983). Compared to continuous injection, cyclic injection tends to promote the development of more fractures in a broader zone. Cerfontaine and Collin (2017) state that during monotonic loading almost all grains along the macroscopic fracture are cracked while cyclic loading leads to failure along grain boundaries and most of the grains stay intact. This observation from mechanical cyclic test and preliminary results from triaxial cyclic tests on Pohang granite cores supports our hypothesis that also in fatigue hydraulic fracturing low energy grain boundary cracks can develop. The division of the injected hydraulic energy into smaller parts is expected to lead to a division of the seismic radiated energy. Another reason for smaller seismic events in hydraulic fatigue is that during the pressure reduction phase the rock mass can relax, which means that induced stresses are reduced and seismic energy is released. After the stress re-distribution, during the following injection cycle the fluid is given the chance to find the new path of least energy (grain boundary) forming a wider fracture network. If and how specific fracture pattern could be designed by special injection schemes remains an open question, but suggests further research on this topic. In terms of economic benefit, fatigue hydraulic fracturing may not be advantageous in the short term due to longer duration of stimulation campaign required. As a cyclic soft stimulation concept, the technique with more operational cost that can control and reduce the magnitude of seismic events (hazard aspect) has an advantage economically in the long term. This is simply because the life time of the project has been extended by applying the hydraulic fatigue treatment.

6 Conclusions

The cyclic progressive and/or pulse injection scheme presented in this study indicate that induced seismicity is manageable in terms of number of events, and distribution of magnitudes of events over injection time. This finding appears to have potentially significant implications for reducing the size of earthquakes in injection processes, which could potentially have a large implication for the reduction of risk (economic and physical) posed to the communities affected by human-induced earthquakes. Caution is necessary, certainly, to translate these implications to projects of different scales and/or in different environments. In this respect, we conclude that our cross-scale approach is beneficial over approaches focusing on laboratory, mine and field scale only.

The fatigue testing scheme with cyclic progressive increase in target pressure, oscillations in the pressurization phases, and frequent interruptions with depressurization phases applied to granitic rock allows for control of hydraulic fracture initiation and propagation. The seismic efficiency is lowered by increasing the number of fatigue cycles and the cumulative hydraulic energy pumped into the rock. In hydraulic fatigue, the permeability enhancement process benefits from a larger fracture process zone caused by arresting and branching fractures. The working hypothesis for this is that less fracture energy is required and less seismic energy is radiated, if the hydraulic fracture propagates through a rock volume which is previously fragmented in fatigue. We conclude:

- (1) Cyclic injection lowers the fracture breakdown pressure (10% at laboratory scale, and 15% at mine scale). A reduction in breakdown pressure has the benefit of using smaller pumps which makes the treatment safer.
- (2) Cyclic injection has the tendency to systematically reduce the magnitude of the largest induced seismic event. Future tests should aim at finding injection parameters that minimize the maximum seismic magnitude. We suggest investigating the effect of fracturing fluid in concert with number of cycles, crack resting pressure during depressurization phases, and duration time, delay and amplitude of pressurization intervals among others.
- (3) Cyclic injection consistently increases the hydraulic performance of the system. The combination of cyclic progressive and pulse hydraulic fracturing provided the best performance of permeability in mine testing.
- (4) Cyclic injection tends to promote the development of more fractures in a broader zone. However, more work is needed to support this conclusion by the analysis of magnitude frequency distribution of seismic events and fracture pattern analysis in-situ after joint conventional and fatigue hydraulic fracturing experiments.
- (5) Cyclic injection decreases the seismic efficiency. Laboratory unconfined tests indicate a decrease of seismic injection efficiency by five orders of magnitude when increasing the number of fatigue cycles by three order of magnitude. These numbers will change when results from cyclic triaxial injection experiments become available.

More work is needed to build confidence on and to refine the concept of fatigue hydraulic fracturing presented in this study not only for granitic but also for other rock types (sandstones, shales), not only in well-known stress conditions but also in unknown stress states, not only for one but also other energy technologies. The cross-scale approach presented in this study is seen valuable to be applied also in subsequent studies.

Acknowledgements

The in-situ experiment at Äspö Hard Rock Laboratory (HRL) was supported by the GFZ German Research Center for Geosciences (75%), the KIT Karlsruhe Institute of Technology (15%) and the Nova Center for University Studies, Research and Development Oskarshamn (10%). We thank Gerd Klee, MeSy Solexperts and Hana Semikova, ISATech Ltd for performing the hydraulic fracturing experiments and Göran Nilsson, GNC for arranging the diamond drillings. We thank Katrin Plenkers and Thomas Fischer (GMuG) for the implementation of acoustic emission sensors and accelerometer, and for managing the continuous and triggered recording system during the hydraulic fracturing experiments. An additional in-kind contribution of the Swedish Nuclear Fuel and Waste Management Co (SKB) for using Äspö HRL as test site for geothermal research is greatly acknowledged.

Hannes Hofmann is currently funded by the EU Horizon 2020 project DESTRESS (Grant agreement No. 691728). Ki Bok Min is supported by the Korea-EU Joint Research Support Program of the National Research Foundation of Korea (NRF) through a grant funded by the Korean Government's Ministry of Science, ICT and Future Planning (No. NRF-2015 K1A3A7A 03074226). We like to thank Graeme Weatherill for commenting an earlier version of this manuscript. Finally, we like to acknowledge the constructive comments and valuable input of two anonymous reviewers and experts in the field of hydraulic fracturing.

References

- Ask D (2006) Measurement-related uncertainties in overcoring data at the Äspö HRL, Sweden. Part 2: Biaxial tests of CSIRO HI overcore samples. *Int. J. Rock Mech. Min. Sci.* 43(1), 127–138
- Atkinson BK (1984) Subcritical crack growth in geological materials. *Journal of Geophysical Research* 89, 4077–4114
- Bachmann CE, Wiemer S, Woessner J, Hainzl S (2011) Statistical analysis of the induced Basel 2006 earthquake sequence: introducing a probability-based monitoring approach for Enhanced Geothermal Systems. *Geophys J Int* 186:793–807. doi: 10.1111/j.1365-246X.2011.05068.x
- Bao X, Eaton DW (2016) Fault activation by hydraulic fracturing in western Canada. *Science*, November 17th
- Bandis SC, Lumsden AC, Barton N (1983) Fundamentals of rock joint deformation. *International Journal of Rock Mechanics Mining Sciences & Geomechanics Abstracts* 20: 249–268
- Block et al. (2014) *Seismological Research Letters* 85, 609–624
- Bommer JJ, Crowley H, Pinho R (2015) A risk-mitigation approach to the management of induced seismicity. *J Seismol* 19:623–646. doi: 10.1007/s10950-015-9478-z
- Bommer JJ, Oates S, Cepeda JM et al. (2006) Control of hazard due to seismicity induced by a hot fractured rock geothermal project. *Eng Geol* 83:287–306. doi: 10.1016/j.enggeo.2005.11.002
- Cerfontaine B, Collin F (2017) Cyclic and fatigue behaviour of rock materials: Review, interpretation and research perspectives. *Rock Mech Rock Eng* DOI 10.1007/s00603-017-1337-5
- Clarke H, Eisner L, Styles P, Turner P (2014) Felt seismicity associated with shale gas hydraulic fracturing: The first documented example in Europe. *Geophysical Research Letters* 41, 8308–8314
- Crane FAA, Furness J (1997) Selection and use of engineering. Elsevier Science and Technology Books, 3rd Edition.
- Davies R, Foulger G, Bindley A, Styles P (2013) Induced seismicity and hydraulic fracturing for recovery of hydrocarbons. *Marine and Petroleum Geology* 45, 171–185
- Ellsworth, W.L., 2013. Injection-induced earthquakes. *Science* 341, <http://dx.doi.org/10.1126/science.1225942>
- Erarslan N, Williams DJ (2012) Mechanism of rock fatigue damage in terms of fracturing rocks. *International Journal of fatigue* 43, 76–89
- Evans, K.F., Zappone, A., Kraft, T., Deichmann, N., Moia, F., 2012. A survey of the induced seismic responses to fluid injection in geothermal and CO2 reservoirs in Europe. *Geothermics* 41, 30–54
- Foulger GR, Wilson MP, Gluyas JG, Julian BR, Davies RJ (2018) Global review of human-induced earthquakes. *Earth-Science Reviews*, <http://dx.doi.org/10.1016/j.earscirev.2017.07.008>
- Friberg PA, Besana-Ostman GM, Dricker I (2014) Characterisation of an earthquake sequence triggered by hydraulic fracturing in Harrison County, Ohio. *Seismological Research Letters* 85, 1295–1307
- Frohlich C (2012) Two-year survey comparing earthquake activity and injection-well locations in Barnett Shale, Texas. *Proc. Natl. Acad. Sci. U.S.A.* 109, 13934–13938
- Ghamgosar M, Erarslan N (2016) Experimental and numerical studies on development of fracture process zone (FPZ) in rock s under cyclic and static loading. *Rock Mechanics Rock Engineering* 49, 893–908
- Giardini D (2009) Geothermal quake risk must be faced. *Nature* 426, 848–849
- Gischig VS, Doetsch J, Maurer H, Krietsch H, Amann F, Evans KF, Nejati M, Jalali M, Valley B, Obermann A, Wiemer S, Giardini D (2017) On the link between stress field and small-scale hydraulic fracture growth in anisotropic rock derived from microseismicity. *Solid Earth Discuss*, <http://doi.org/10.5194/se-2017-78>
- Goodfellow SD, Nasser MHB, Maxwell SC, Young RP (2015), Hydraulic fracture energy budget: Insights from the laboratory, *Geophys. Res. Lett.* 42(9), 3179–3187, 820 doi:10.1002/2015GL063093
- Grünthal G (2014) Induced seismicity related to geothermal projects versus natural tectonic earthquakes and other types of induced seismicity events in Central Europe. *Geothermics* 52, 22–35
- Guglielmi Y, Cappa F, Avouac J-P, Henry P, Elsworth D (2015) Seismicity triggered by fluid injection-induced aseismic slip. *Science* 346, Issue 6240, 1224–1226

- Häring MO, Schanz U, Ladner F, Dyer BC (2008) Characterization of Basel 1 enhanced geothermal system. *Geothermics* 37, 469–495
- Haimson BC, Kim CM (1991) Mechanical behaviour of rock under cyclic fatigue. *Rock Mechanics* 3, 845–863
- Haimson BC, Cornet F (2003) ISRM Suggested Methods for rock stress estimation-Part 3: hydraulic fracturing (HF) and/or hydraulic testing of pre-existing fractures (HTPF). *Int. J. Rock Mech. Min. Sci.* 40(7–8), 1011–1020
- Hofmann H, Zimmermann G, Zang A, Farkas M, Huenges E, Min KB, Park S, Kim K, Fokker P, Westaway R, Bethmann F, Meier P, Guinot F, Yoon KS, Choi J, Jeong U, Han YH, Lee TJ, Song YH, Kim MS, Yoon BJ, Lee KS, Kim KY (2017) First field application of a cyclic injection protocol and an advanced traffic light system to mitigate the seismic risk from hydraulic stimulation at the Pohang Enhanced Geothermal System project site in Korea. 12th EURO-conference on Rock Physics and Geomechanics – Bridging between Rock Physics and Structural Geology. Ma'ale HaHamisha, Israel, 5-10 November 2017.
- Indamdar A et al. (2010) Evaluation of stimulation techniques using microseismic mapping in the eagle Ford shale. Society Petroleum Engineers, SPE 136873
- Jiráková H, Frydrych V, Vintera J, Krásný O, Vanecek M (2015) Results of the rock hydraulic fracturing research project. *Tunel - Undergr. Constr. Mag. Czech Tunneling Assoc. Slovak Tunneling Assoc.*, 24(4), 57–64
- Keranen KM, Weingarten M, Abers GA, Bekins A, Ge S (2014) Sharp increase in central Oklahoma seismicity since 2008 induced by massive wastewater injection. *Science* 345, 448–451
- Khazaei C, Hazzard J, Chalaturnyk R (2015) Damage quantification of intact rocks using acoustic emission energies recorded during uniaxial compression test and discrete element modeling. *Computers and Geotechnics* 67, 94–102
- Kiel OM (1977) Kiel process reservoir stimulation by dentritic fractures. Society Petroleum Engineers AIME, Paper SPE 6984-MS
- Kim WY (2013) Induced seismicity associated with fluid injection into deep well in Youngstown, Ohio. *Journal of Geophysical Research* 118, 3506–3518
- Klee G, Rummel F (2002) Rock stress measurements at the Äspö HRL Hydraulic fracturing in boreholes, Technical Report IPR-02-02, Stockholm, SKB
- Kwiatek G, Plenkens K, Martinez Garzon P, Leonhardt M, Zang A, Dresen G (2017a) New Insights into Fracture Process through In-Situ Acoustic Emission Monitoring during Fatigue Hydraulic Fracture Experiment in Äspö Hard Rock Laboratory. - *Procedia Engineering*, 191, 618–622
- Kwiatek et al. (2017b) Insights into complex sub-decimeter fracturing processes occurring during a water-injection experiment at depth in Äspö Hard Rock Laboratory, Sweden. *Journal of Geophysical Research*, submitted
- Lopez Comino J, Heimann S, Cesca S, Milkereit C, Dahm T, Zang A (2017a) Automated Full Waveform Detection and Location Algorithm of Acoustic Emissions from Hydraulic Fracturing Experiment. - *Procedia Engineering*, 191, 697–702
- Lopez Comino J, Heimann S, Cesca S, Grigoli F, Milkereit C, Dahm T, Zang A (2017b) Characterization of hydraulic fractures growth during the Äspö Hard Rock Laboratory Experiment (Sweden), *Rock Mech Rock Eng* 50, 2985–3001
- Lockner DA, Byerlee JD, Kukusenko V, Ponomareva A, Sidorin A (1991) Quasi-static fault growth and shear fracture energy in granite. *Nature* 350, 39–42
- Maxwell SC, Schemata J, Campbell E, Quirk D (2008), Microseismic deformation rate monitoring, paper presented at SPE Annual Technical Conference and Exhibition, SPE–116596-MS, Denver, Colo., 21–24 Sept
- Maxwell SC, Jones M, Parker R, Miong S, Leaney S, Dorval D, D'Amico D, Logel J, Anderson E, Hammermaster K (2009) Fault Activation During Hydraulic Fracturing. SEG Houston 2009 International Exposition and Annual Meeting 1552e1556
- Maxwell, SC (2013), Unintentional seismicity induced by hydraulic fracturing, *CSEG Rec. - Focus Artic.* 38(8)
- Maxwell SC, Zhang F, Damjanac B (2015) Geomechanical modeling of induced seismicity resulting from hydraulic fracturing. *Leading Edge*, 34(6), 678–683
- McGarr (1976) Seismic moments and volume changes. *Journal of Geophysical Research* 81(1), 1487–1494
- McGarr A (2014) Maximum magnitude earthquakes induced by fluid injection. *Journal of Geophysical Research Solid Earth* 119, 1008–1019. doi:10.1002/2013JB010597
- McGarr A, Bekins B, Burkard N, Dewey J, Earle P, Ellsworth W, Ge S, Hickman S, Holland A, Majer E, Rubinstein J, Sheehan A (2015) Coping with earthquakes induced by fluid injection. *Science* 347, Issue 6224, 830–831
- McMahon ND et al. (2017) Spatiotemporal evolution of the 2011 Prague, Oklahoma, aftershock sequence revealed using subspace detection and relocation. *Geophysical Research Letters* 44, 7149–7158
- Majer E, Nelson J, Robertson-Tait A, Savy J, Wong I, 2012. Protocol for addressing induced seismicity associated with enhanced geothermal systems. U.S. Department of Energy; Report No.: DOE/EE-0662
- Mena B, Wiemer S, Bachmann C (2013) Building robust models to forecast induced seismicity related to geothermal reservoir enhancement. *Bull Seismol Soc Am* 103:383–393. doi: 10.1785/0120120102
- Nichols TC (1975) Deformation associated with relaxation of residual stresses in a sample of Barre granite from Vermont, Prof. Pap. US Geol. Sum. 875, 32 pages
- Paris PC, Erdoan F (1967) *J. Bas. Eng., Trans. ASME Series D*, 89, 459
- Patel SM, Sondergeld CH, Rai CS (2017) Laboratory studies of hydraulic fracturing by cyclic injection. *International Journal of Rock Mechanics and Mining Sciences* 95, 8–15
- Rubinstein JL, Mahani AB (2015) Myths and Facts on wastewater injection, hydraulic fracturing, enhanced oil recovery, and induced seismicity. *Seismol. Res. Lett.*, 86(4), 1060–1067
- Rutqvist J, Rinaldi AP, Cappa F, Moridis GJ (2013) Modeling of fault reactivation and induced seismicity during hydraulic fracturing of shale-gas reservoirs. *J Pet Sci Eng* 107:31–44. doi:10.1016/j.petrol.2013.04.023
- Rutqvist J, Rinaldi AP, Cappa F, Moridis GJ (2015) Modeling of fault activation and seismicity by injection directly into a fault zone associated with hydraulic fracturing of shale-gas reservoirs. *J Pet Sci Eng* 127:377–386. doi:10.1016/j.petrol.2015.01.019
- Safari R, Gandikota R, Mutlu O, Missy J, Glanville J, Abass H (2015) Pulse fracturing in shale reservoirs: Geomechanical aspects, ductile/brittle transition, and field implications. Paper SPE 168759, December SPE Journal 1287–1304
- Suckale J (2009) Induced seismicity in hydrocarbon fields, *Advances Geophys.* 51, 55–106
- Swift RP, Kusubov AS (1982) Multi fracturing of boreholes by using tailored-pulse loading. Paper SPE 9892-PA, SPE Journal 22(6), 923–932
- Vogler D, Amann F, Bayer P, Elsworth D (2016) Permeability Evolution in Natural Fractures Subject to Cyclic Loading and Gouge Formation. *Rock Mech Rock Engng* 49(9), 3463–3479.

- Wang R, Gu YJ, Schultz R, Kim A, Atkinson G (2016) Source analysis of a potential hydraulic-fracturing-induced earthquake near Fox Creek, Alberta. *Geophysical Research Letters* 43, 564-573
- Wang J, Ellsworth D, Wu Y, Liu J, Zhu W, Liu Y (2018) The influence of fracturing fluids on fracturing processes: A comparison between water, oil and SC-CO₂. *Rock Mech Rock Eng* 51, 299-313
- Warpinski NR, Du J, Zimmer U (2012) Measurements of Hydraulic-Fracture-Induced Seismicity in Gas Shales. *SPE Production and Operations*, pp. 240–252
- Warpinski NR (2013), Understanding hydraulic fracture growth, effectiveness, and safety through microseismic monitoring. In: *Effective and Sustainable Hydraulic Fracturing*, p. 10.5772/55974
- Weingarten et al. (2015) High-rate injection is associated with increase in U.S. mid-continent seismicity. *Science*, Vol. 348, Issue 6241, 1336-1340
- Westaway R, Younger PL (2014) Quantification of potential macroseismic effects of the induced seismicity that might result from hydraulic fracturing for shale gas exploitation in the UK. *Quarterly Journal of engineering Geology and Hydrology* 47, 333-350.
- Wilson, M. P., Worrall F, Davies R.J., Almond S, (2018) Fracking: How far from faults? *Geomechanics and Geophysics for Geo-Energy and Geo-Resources* <https://doi.org/10.1007/s40948-018-0081-y>.
- Wolhart SL, Harting TA, Dahlem JE, Young TJ, Mayerhofer MJ, Lolon EP (2005) Hydraulic fracture diagnostics used to optimize development in the Jonah Field. *SPE* 102528
- Xu J, Zhai C, Qin L (2017) Mechanism and application of pulse hydraulic fracturing in improving drainage of coalbed methan. *Journal of Natural Gas Science and Engineering* 40, 79-90
- Yeck WL, Block LV, Wood CK, King VM (2015) Maximum magnitude estimations of induced earthquakes at Paradox Valley, Colorado, from cumulative injection volume and geometry of seismicity clusters. *Geophysical Journal International* 200, 322-336
- Yoon JS, Zang A, Stephansson O (2014) Numerical investigation on optimized stimulation of intact and naturally fractured deep geothermal reservoirs using hydro-mechanical coupled discrete particles joints model, *Geothermics* 52:165–184
- Yoon JS, Zang A, Zimmermann G (2015a) Numerical investigation on stress shadowing in fluid injection-induced fracture propagation in naturally fractured geothermal reservoir. *Rock Mechanics and Rock Engineering*, Vol. 48, 1439-1454
- Yoon JS, Zimmermann G, Zang A, Stephansson O (2015b), Discrete element modeling 985 of fluid injection-induced seismicity and activation of nearby fault, *Can. Geotech. J.* 52(10), 1457–1465, doi:10.1139/cgj-2014-0435
- Yoon JS, Zimmermann G, Zang A (2015c) Discrete element modeling of cyclic rate fluid injection at multiple locations in naturally fractured reservoirs. *International Journal of Rock Mechanics and Mining Sciences* 74, 15-23
- Yoon JS, Zang A, Stephansson O, Hofmann H, Zimmermann G (2017) Discrete element modelling of hydraulic fracture propagation and dynamic interaction with natural fractures in hard rock. *Procedia Engineering*, 191: 1023–1031
- Zang A, Wagner FC, Stanchits S, Janssen, C, Dresen G (2000) Fracture process zone in granite. *Journal of Geophysical Research*, Vol. 105, B10, 23651-23661
- Zang A, Stanchits S, Dresen G (2002) Acoustic emission controlled triaxial rock fracture and friction tests. In: Dyskin, A.V., Hu, X. & Sahouryeh, E. (eds.), *Structural Integrity and Fracture*, Swets & Zeitlinger, Lisse, pp 289-294
- Zang A, Stephansson O (2010) *Stress field of the Earth's crust*. Dordrecht, Springer
- Zang, A., J. S. Yoon, O. Stephansson, and O. Heidbach (2013), Fatigue hydraulic fracturing by cyclic reservoir treatment enhances permeability and reduces induced seismicity. *Geophys. J. Int.* 195(2), 1282–1287, doi:10.1093/gji/ggt301. 993
- Zang A, Oye V, Jousset P, Deichmann N, Gritto R, McGarr A, Majer E, Bruhn D (2014), Analysis of induced seismicity in geothermal reservoirs – An overview, *Anal. Induc. Seism. Geotherm. Oper.*, 52(0), 6–21, doi:10.1016/j.geothermics.2014.06.005. 996
- Zang A, Stephansson O, Stenberg L, Plenkers K, Specht S, Milkereit C, Schill E, Kwiatek G, Dresen G, Zimmermann G, Dahm T, Weber M (2017a) Hydraulic fracture monitoring in hard rock at 410 m depth with an advanced fluid-injection protocol and extensive sensor array. *Geophys J Int* 208 (2): 790–813
- Zang A, Stephansson O, Zimmermann G (2017b), Keynote: Fatigue Hydraulic Fracturing, *ISRM Eur. Rock Mech. Symp. EUROCK 2017*, 191, 1126–1134, 1001 doi:10.1016/j.proeng.2017.05.287
- Zangeneh N, Eberhardt E, Bustin RM (2015) Investigation of the influence of natural fractures and in situ stress on hydraulic fracture propagation using a distinct-element approach, *Can Geotech J*, 52: 926–946
- Zhang F, Damjanac B, Huang H (2013) Coupled discrete element modeling of fluid injection into dense granular media, *J Geophys Res Sol Earth*, 118: 2703–2722
- Zhou ZL, Zhang GQ, Dong HR, Liu ZB, Nie YX (2017) Creating a network of hydraulic fractures by cyclic pumping. *International Journal of Rock Mechanics and Mining Sciences* 97, 52-63
- Zhuang L, Kim KY; Jung SG, Diaz MB; Min KB, Park S; Zang A, Stephansson O, Zimmerman G, Yoon JS (2016) Laboratory study on cyclic hydraulic fracturing of Pocheon granite in Korea. *American Rock Mechanics Association*, paper ARMA-2016-16
- Zhuang L, Kim KY; Jung SG, Nam YJ; Min KB, Park S; Zang A, Stephansson O, Zimmerman G, Yoon JS (2017) Laboratory evaluation of induced seismicity reduction and permeability enhancement effects of cyclic hydraulic fracturing. *American Rock Mechanics Association*, paper ARMA-2017-757
- Zhuang L, Kim KY, Jung SG, Diaz M, Min KB, Park S, Zang A, Stephansson O, Zimmerman G, Yoon JS (2018) Cyclic hydraulic fracturing of cubic granite samples under triaxial stress state with acoustic emission, injectivity and fracture measurements. *American Rock Mechanics Association*, paper ARMA (submitted)
- Zimmermann G, Moeck I, Blöcher G (2010) Cyclic waterfrac stimulation to develop an enhanced geothermal system (EGS): Conceptual design and experimental results. *Geothermics* 39, 59–69
- Zimmermann G et al. (this issue) Permeability enhancement and fracture development of hydraulic fracturing experiments in the Äspö Hard Rock Laboratory, Sweden
- Zoback, MD (2007) *Reservoir Geomechanics*, Cambridge University Press, Cambridge

Figure Captions

Fig. 1 Summary of relationship between maximum observed seismic magnitudes and fluid volume injected in different field experiments. Symbols indicate geothermal, shale gas, wastewater disposal and KTB deep fluid injection experiment. Colour indicates in situ stress regime at target depth (*red* = normal faulting, *purple* = strike slip, *blue* = thrust faulting regime). Upper bound is the linear relationship postulated by McGarr et al. (2014). Lower bound values come from the extended EGS data base published by Zang et al. (2014).

Fig. 2 Scheme of pumping used in the FHF treatment. (a) Pressure, flow chart of test with four cycles and increasing target pressure, and (b) detail of the progressive cycle 3 at breakdown. The dynamic pulsing (here 5 Hz) applied during the pressurization levels is to disintegrate the rock and remove weak material from fracture faces acting as natural proppants to change the stress field in subsequent cycles of pressurization and depressurization.

Fig. 3 Synoptic view of the fracture process zone resulting from (a) conventional hydraulic fracturing with monotonic increase of injection pressure, and (b) fatigue hydraulic fracturing with frequent phases of depressurization and oscillating pulses during pressurization phases. In (b) rock chips removed from fracture faces through high frequency vibrations (secondary pump) and washed out to the fracture tip allow a change in the local stress field in depressurization phases of the FHF treatment. A larger fracture process zone is created (b), compared to the case with continuous fluid injection in conventional hydraulic fracturing (a).

Fig. 4 Laboratory equipment for hydraulic fracturing at KICT: (a) Control unit, (b) hydraulic pump, (c) tri-axial cell, and (d) interior view of the working table of the industrial X-ray CT scanning used.

Fig. 5 Hydraulic fracture design and high-frequency sensor monitoring network at 410 m depth in Äspö HRL. (a) View of the horizontal hydraulic fracturing borehole F1 drilled in the orientation of Sh. Colour coded disks along F1 indicate locations of mid injection intervals. Monitoring boreholes left and right of the fracturing borehole F1 are equipped with AE sensors. Short boreholes in tunnel roofs are equipped with both, AE sensors and accelerometers. (b) Installing a chain of AE sensors in one of the inclined monitoring boreholes in tunnel TASN.

Fig. 6 Breakdown pressure and maximum event amplitude during five monotonic and twenty cyclic injection tests of Pocheon granite core samples. Dashed lines indicate average values of monotonic and cyclic tests, respectively.

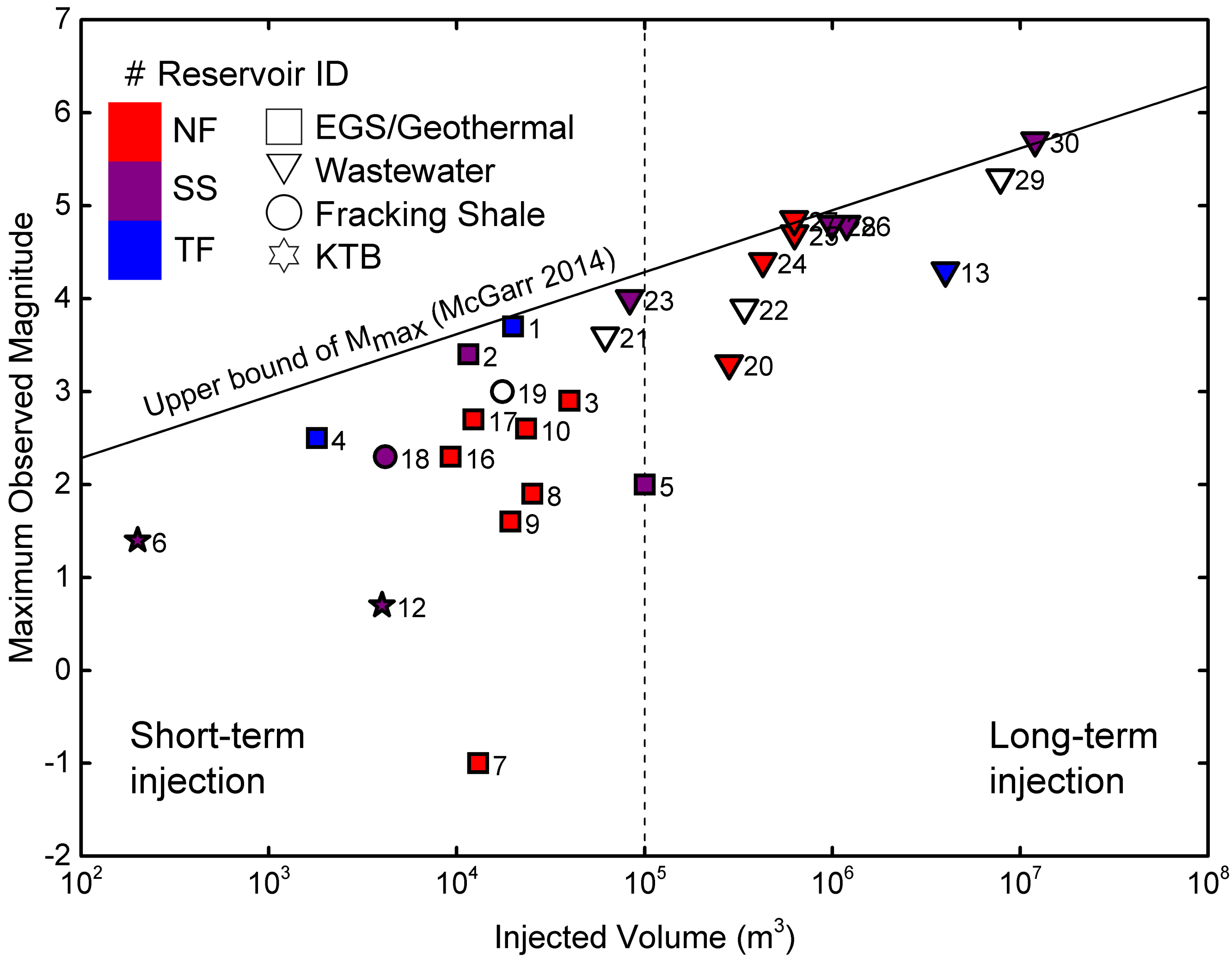
Fig. 7 Visualized fracture pattern of granite cores after monotonic and cyclic injection. (a) X-ray CT images, and (b) fracture only images.

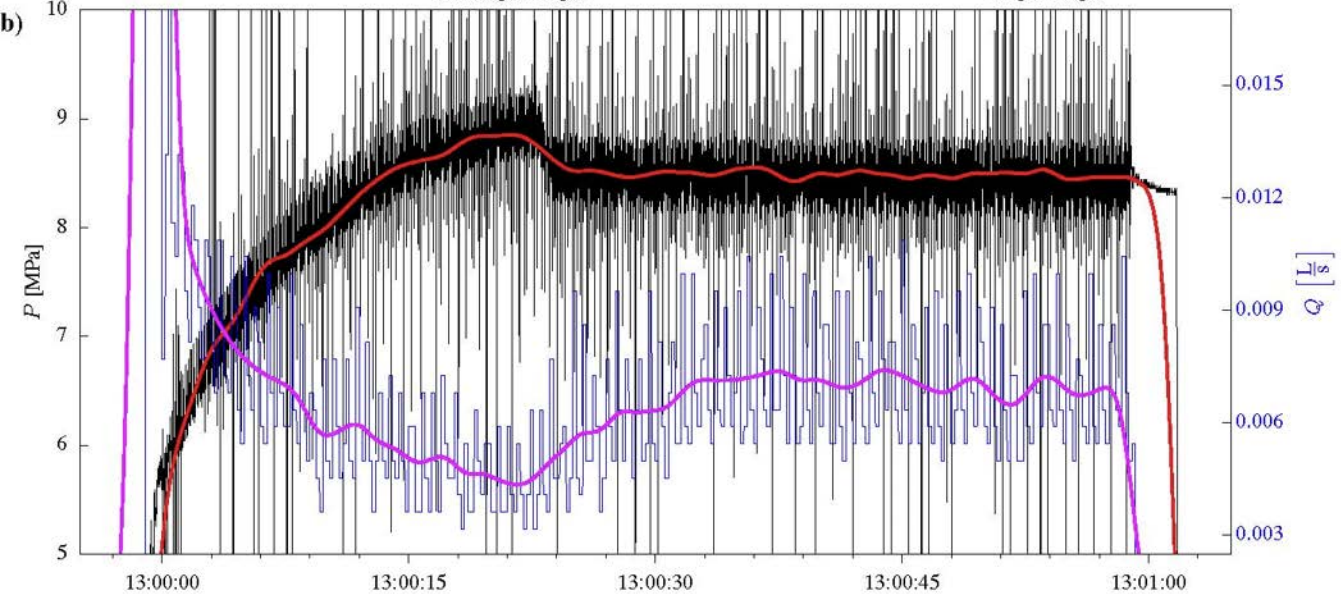
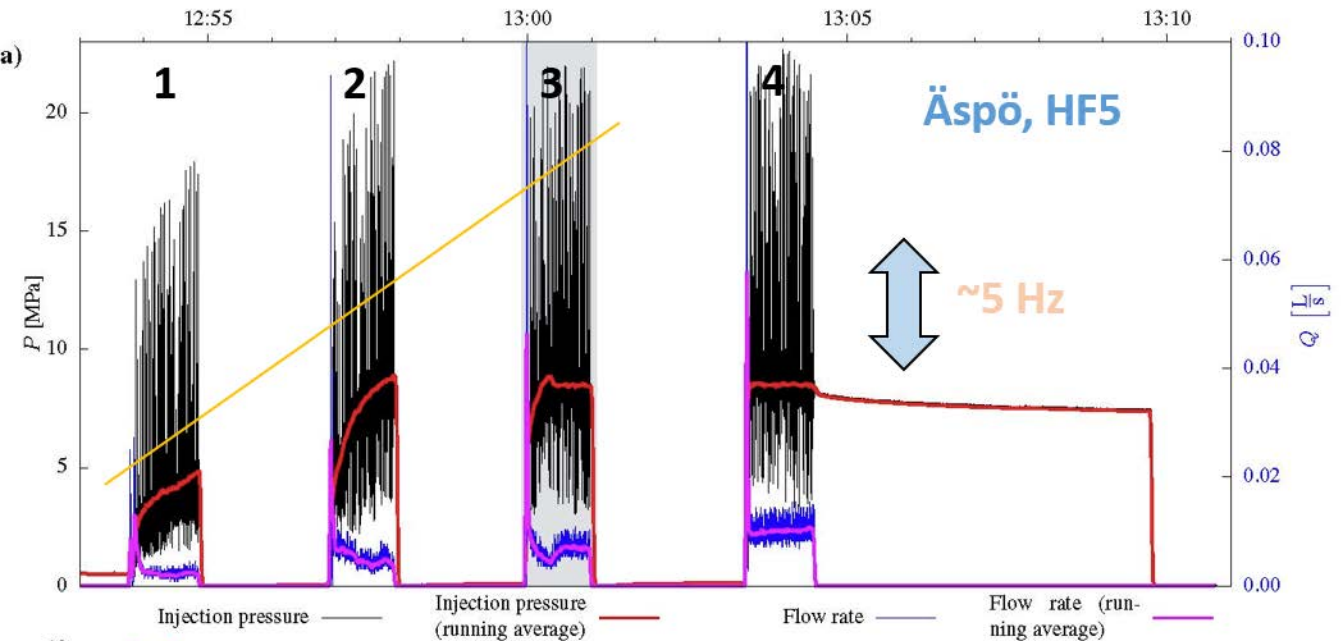
Fig. 8 Number of localized seismic events is shown per fracturing stage for six hydraulic tests in horizontal borehole F1 at 410 m depth in Äspö HRL. Seismicity associated with hydraulic fracture initiation and propagation is sensitive to rock type, fracturing stage and the fluid-injection scheme used. In each experiment, the fracture breakdown pressure, the fracture reopening pressure, the flow rate range, and total volume of water injected is listed right below the experiments identification number (HF1-HF6). The first test, HF1 starts in the deeper part of the 28 m long, horizontal borehole (25 m), and the last test HF6, is operated about 5 m from the onset of F1 at the tunnel wall.

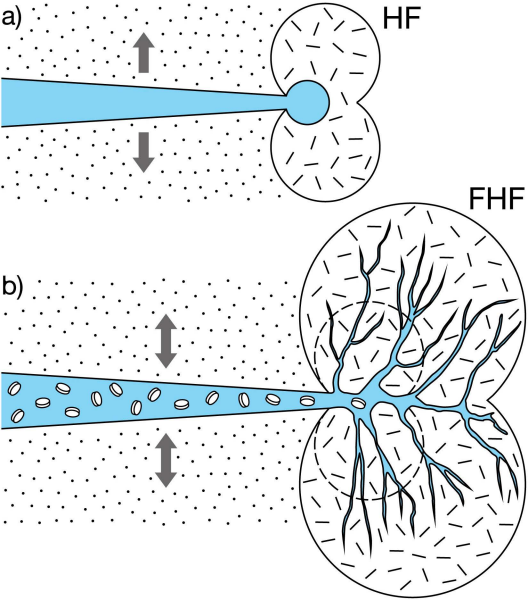
Fig. 9 Locations of 197 AE hypocentres (colour spheres) from six hydraulic testing intervals (colour disks) viewed in the direction of maximum horizontal stress at 410 m depth in Äspö HRL (Kwiatek et al. 2017b, snapshot of movie). In the conventional tests with green (HF1), blue (HF2) and yellow injection intervals (HF6) the AE hypocentres form a planar structure (colour dots). In experiment HF3 with progressive CHF, a cloud of AE is observed. Length of horizontal testing borehole F1 with colour disks is 28 m. AE magnitude is indicated by the size of the color spheres.

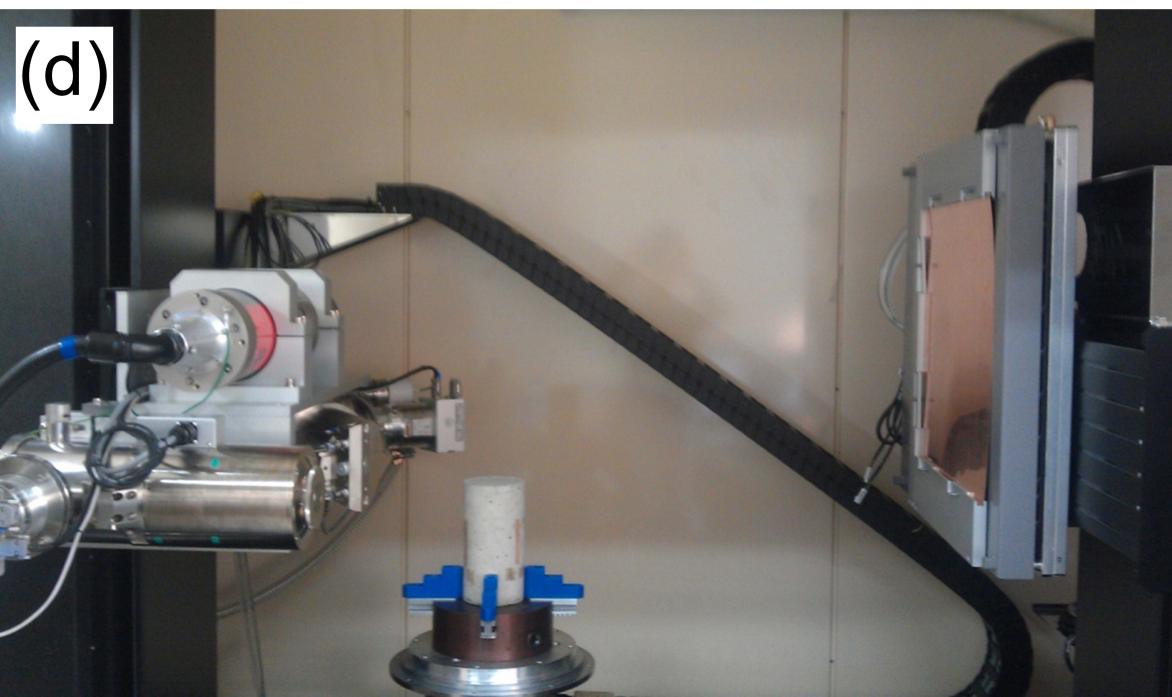
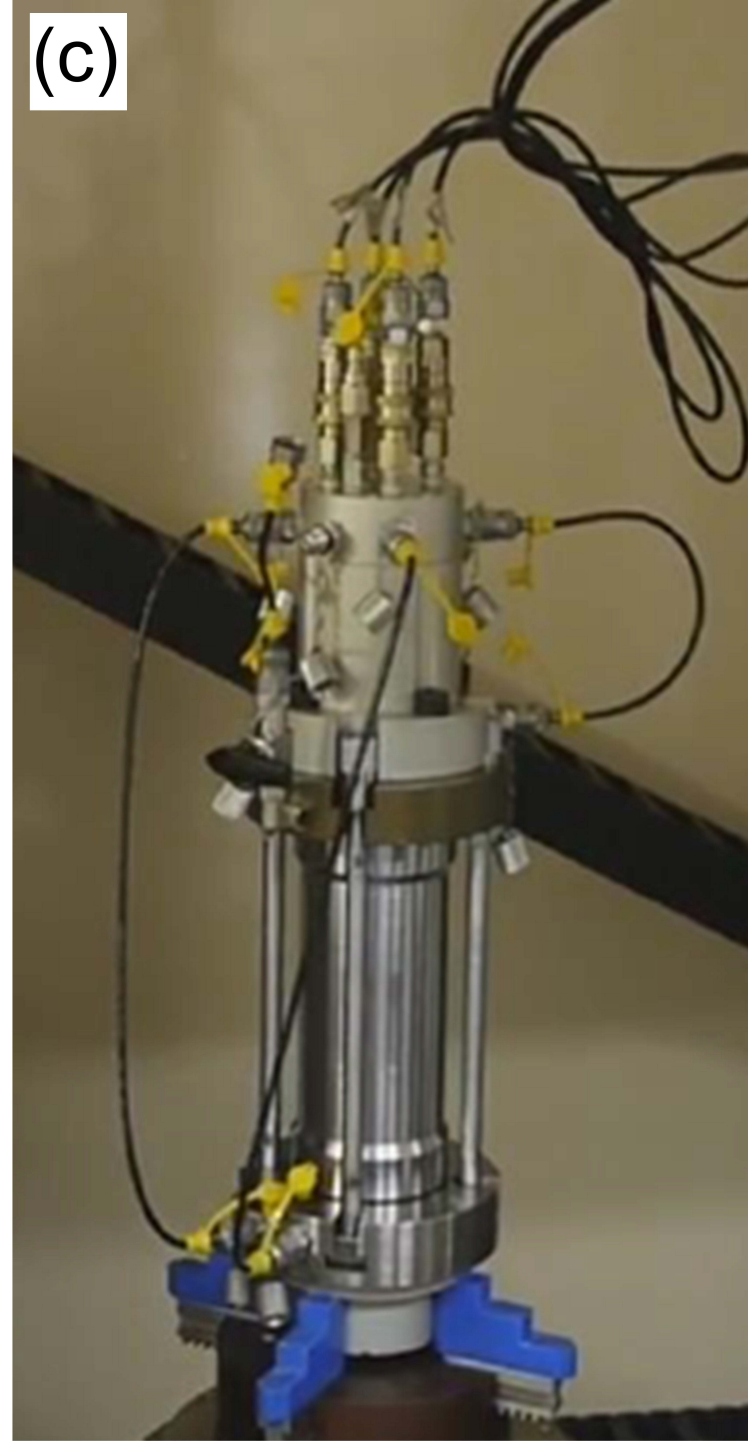
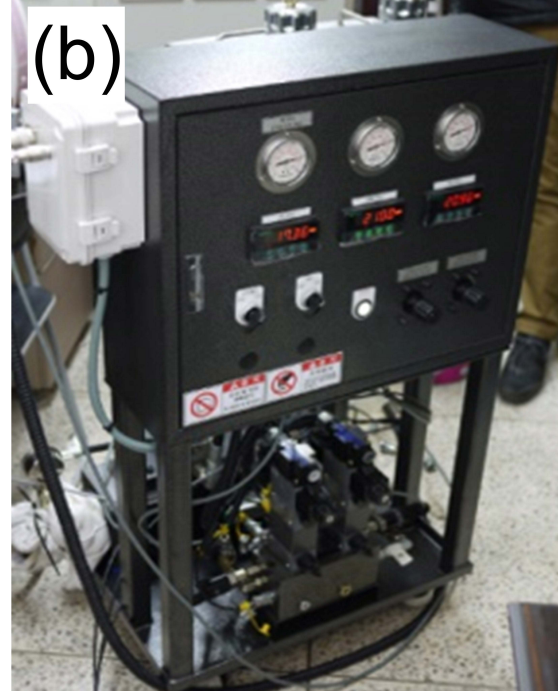
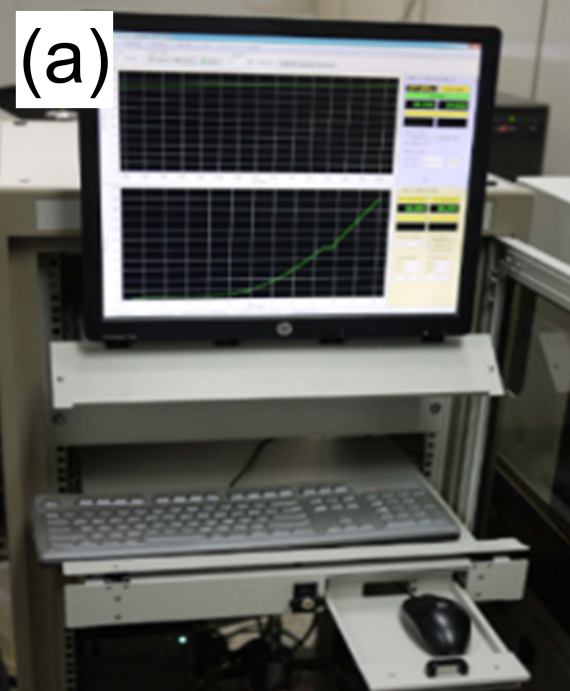
Fig. 10 Permeability enhancement process (upper panel) and seismic activity according to injection style flow rate and pressure chart (lower panel). (a) Experiment HF2 with continuous water injection, and (b) experiment HF3 with cyclic, progressive water injection. Absolute permeability is indicated on left ordinate, and relative permeability is indicated on right ordinate of upper panel view graphs.

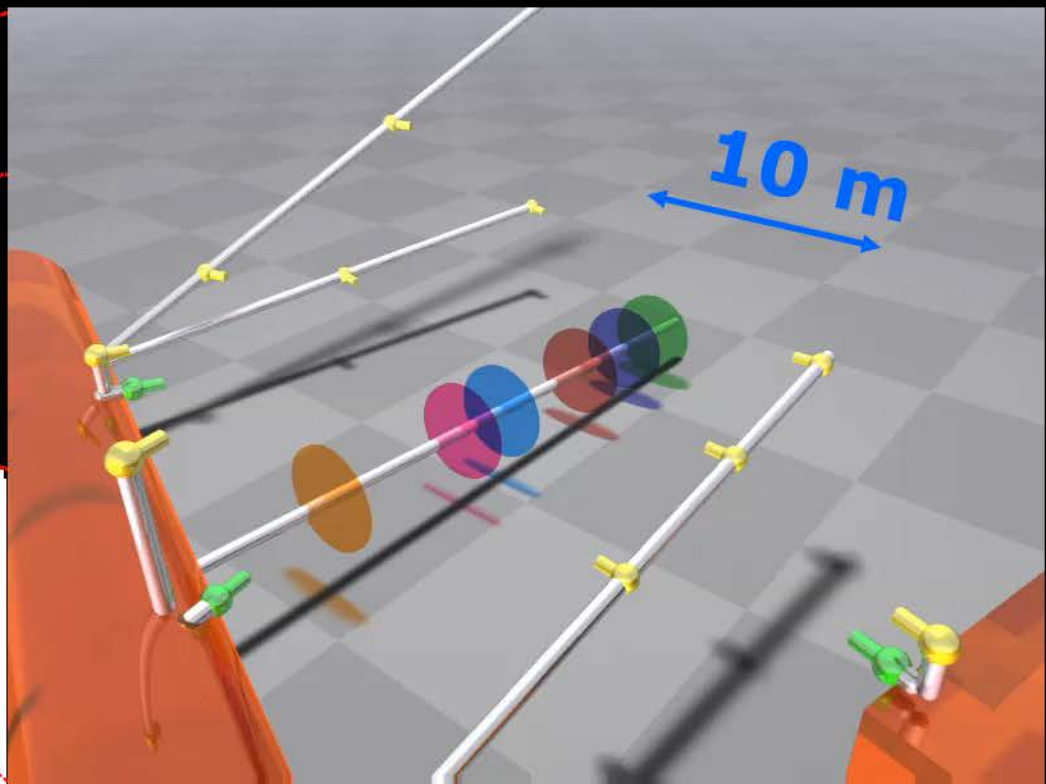
Fig. 11 Seismic injection efficiency plotted against hydraulic energy from laboratory and mine-scale fluid injection experiments. *Circles* refer to laboratory core testing (injection borehole diameter 8 mm) and *diamonds* refer to Äspö HRL underground testing at 410 m depth (injection borehole diameter 102 mm). The number of fatigue hydraulic fracturing cycles is indicated by colour, and ranges from 1 to 839 cycles. For reference, conventional tests with continuous fluid-injection are indicated by open symbols.

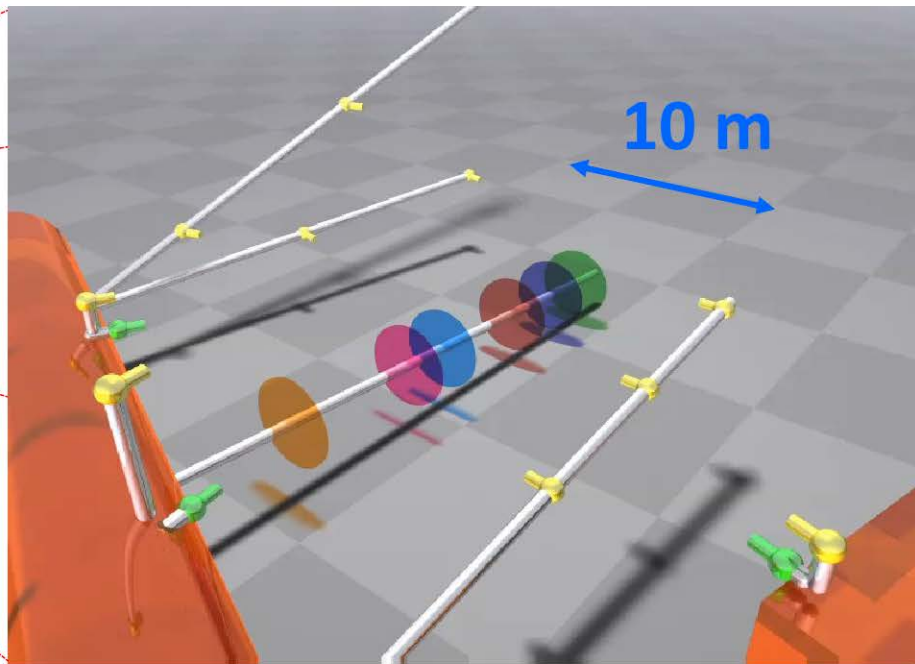
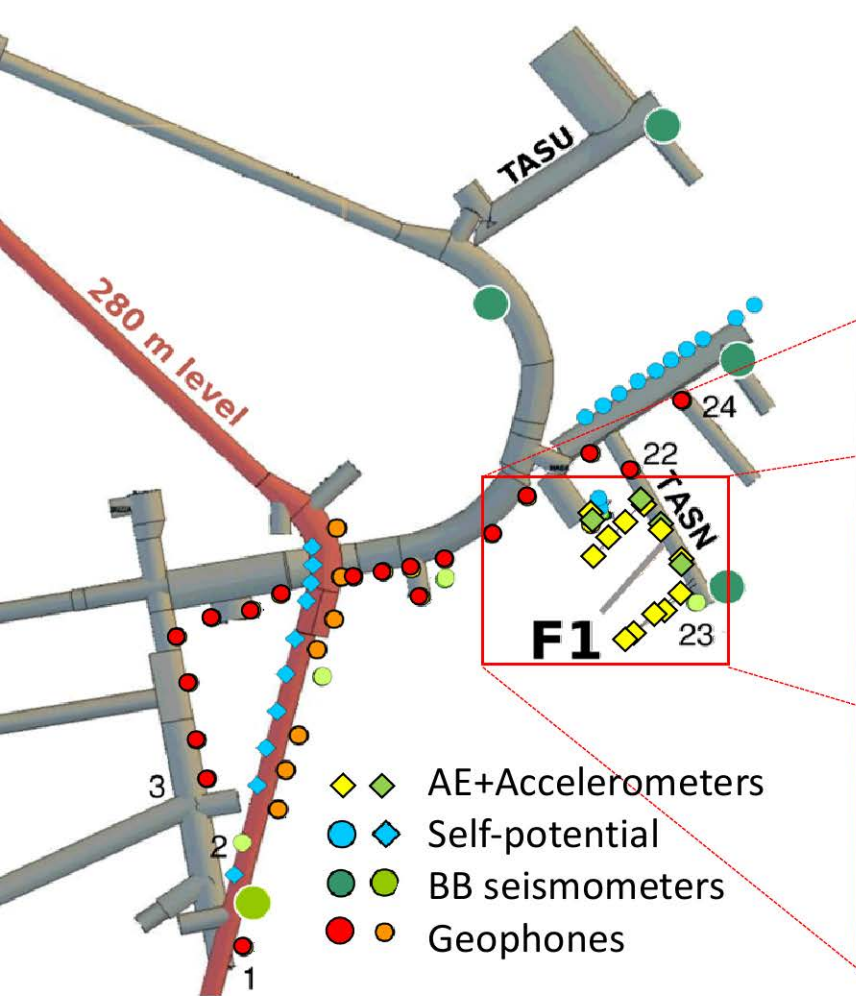




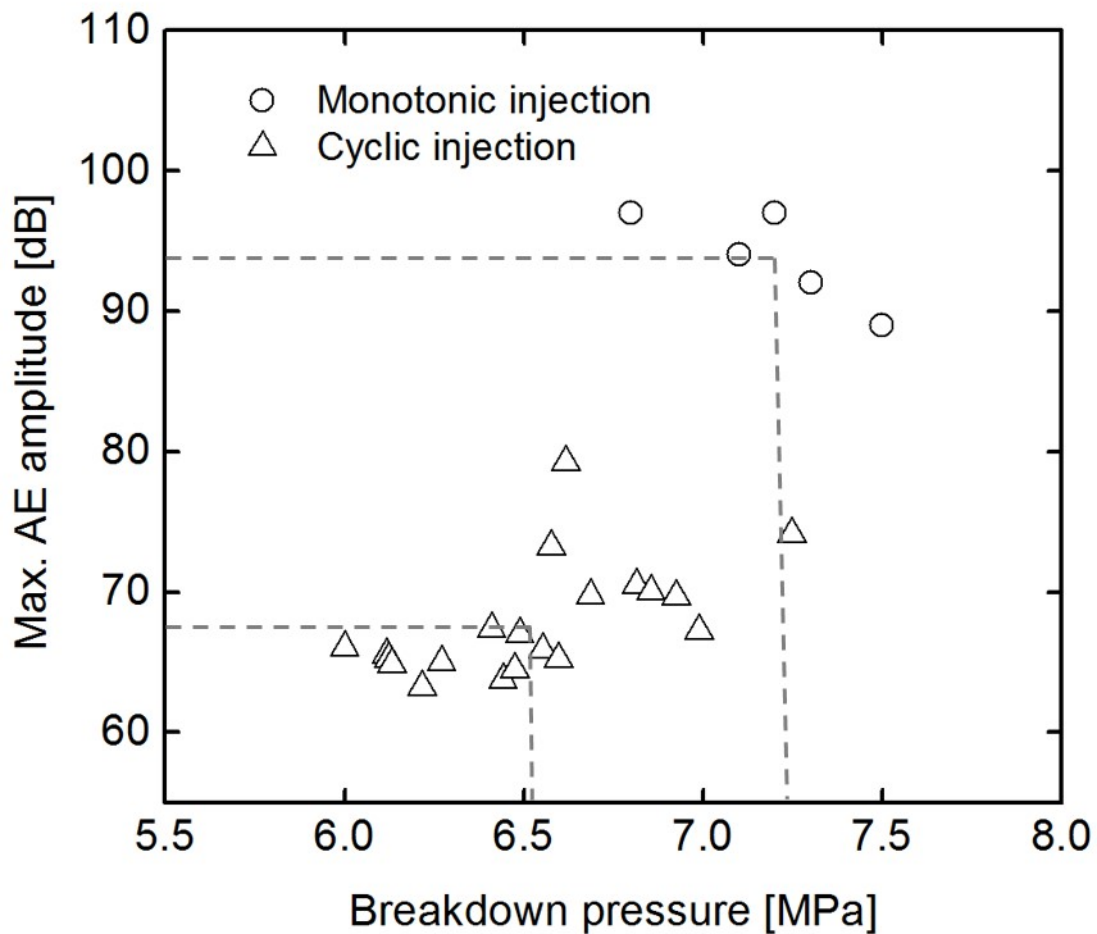








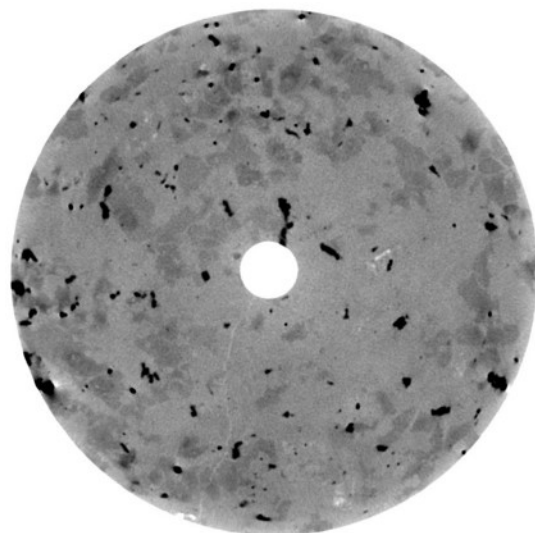




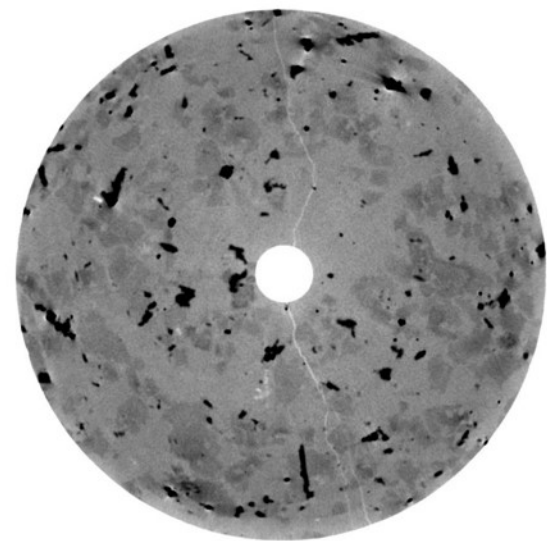
a)



Monotonic

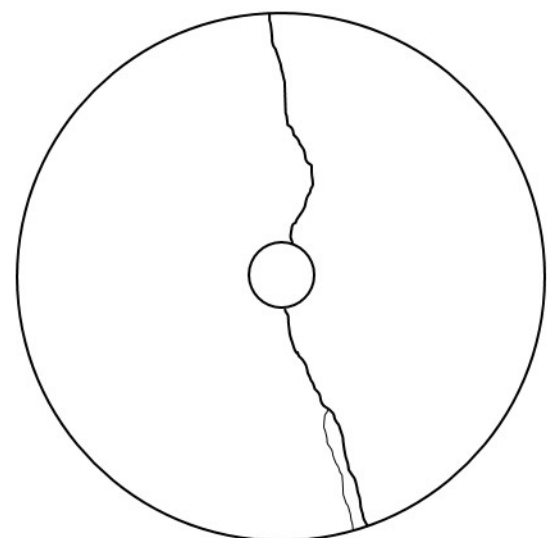
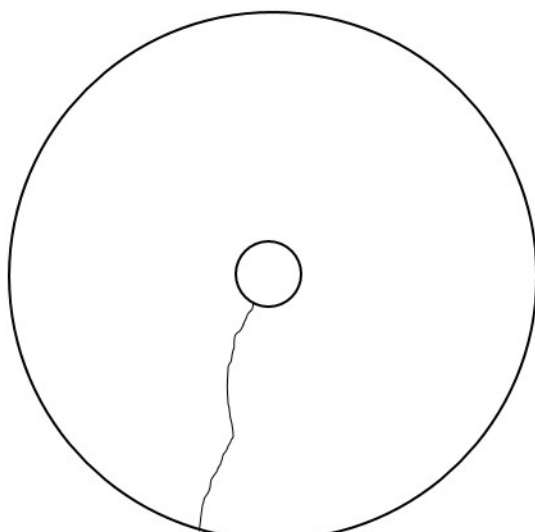
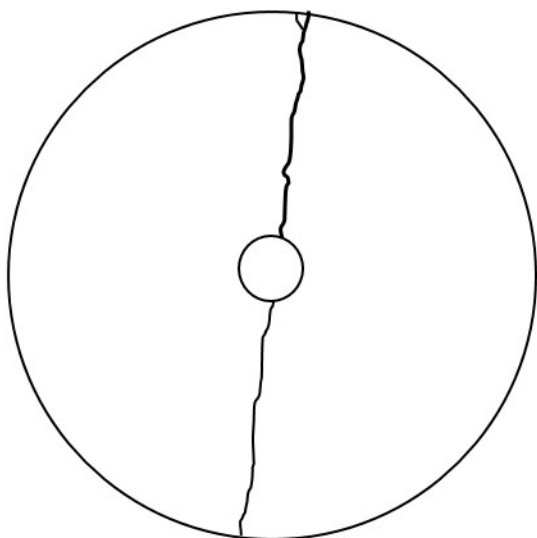


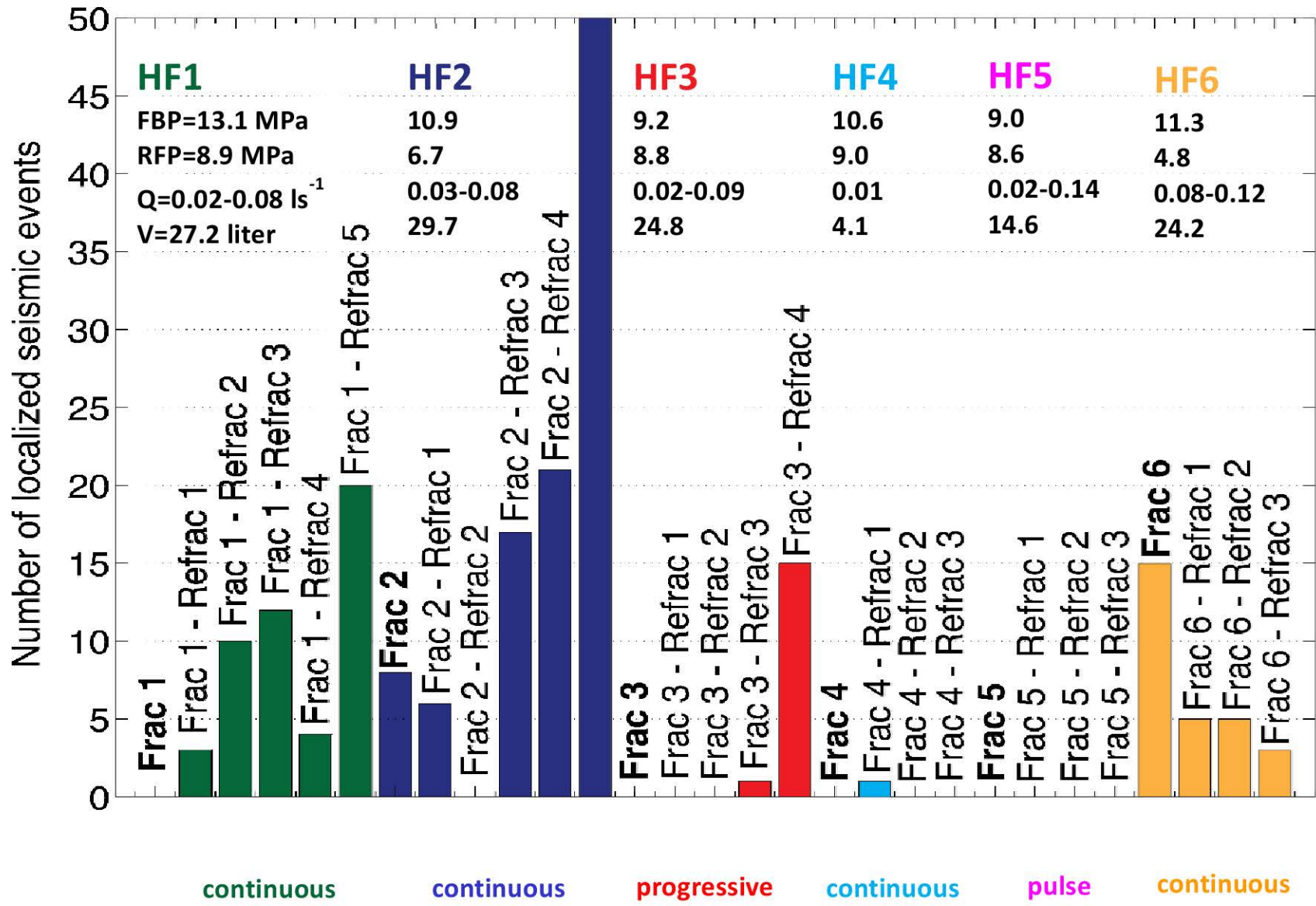
473 cycles



839 cycles

b)

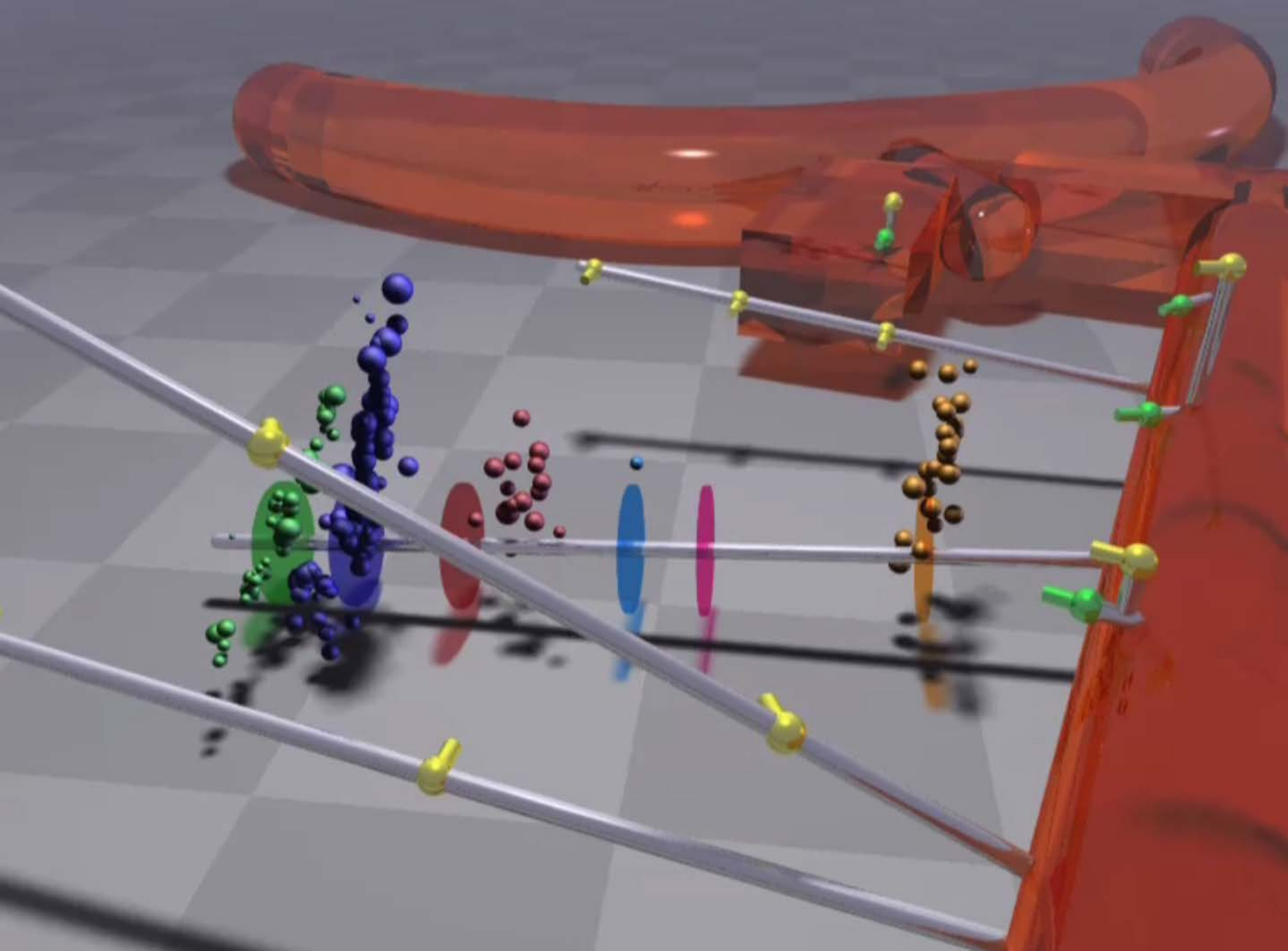


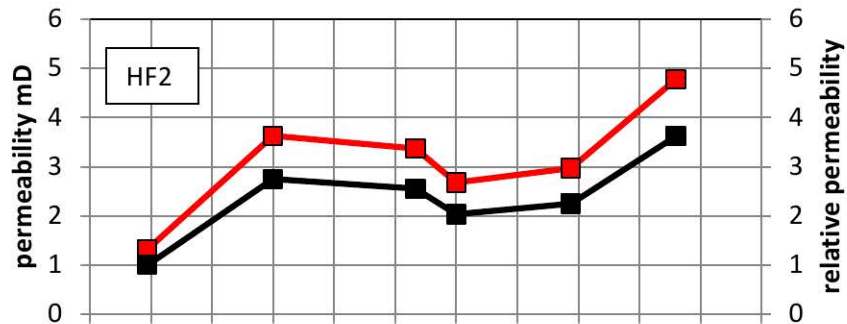
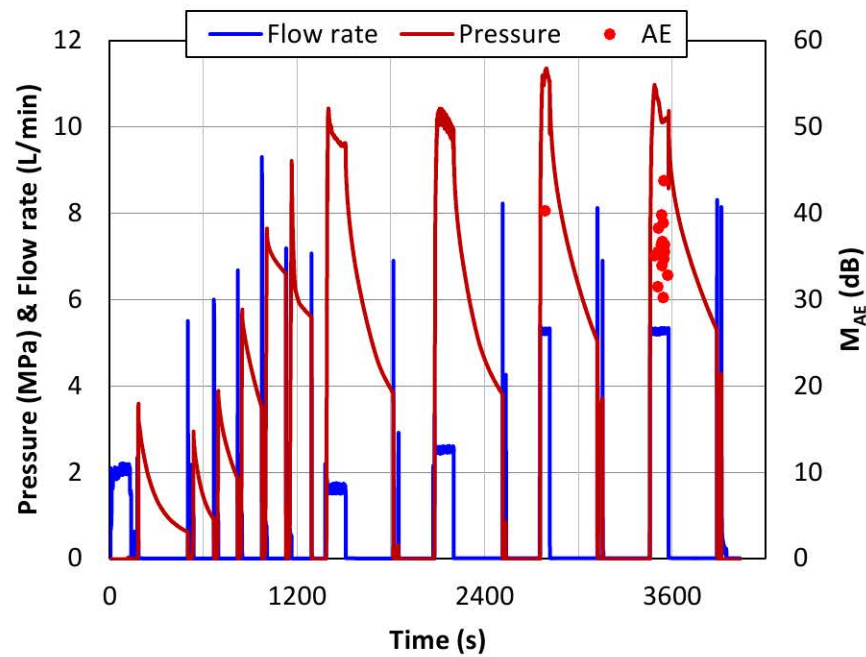
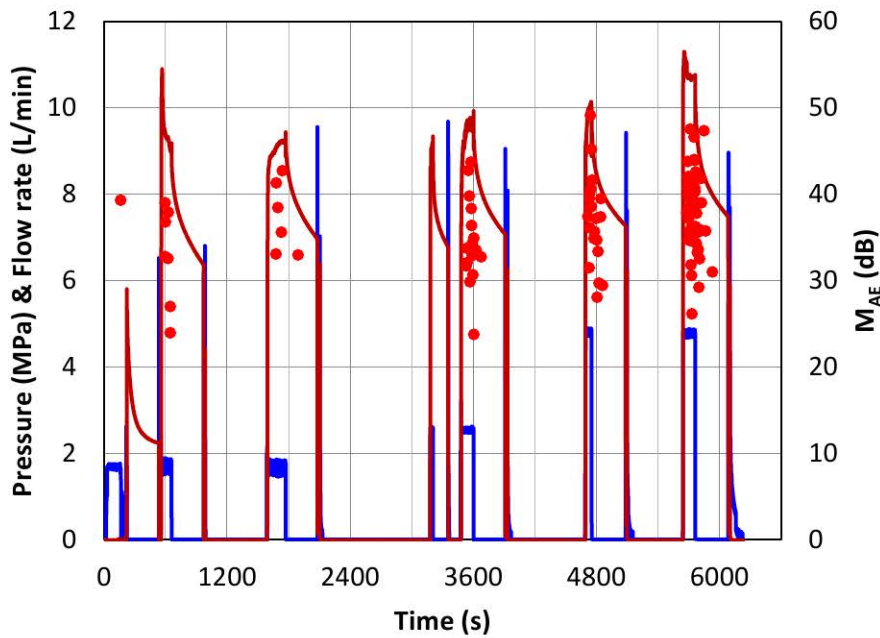
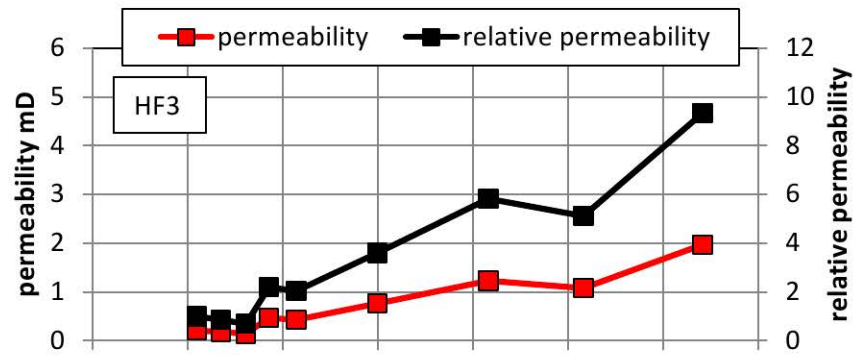


Ävrö granodiorite

diorite-gabbro

granite



(a)**(b)**

Injection Efficiency

